Annual Review of Earth and Planetary Sciences

Dynamic Topography and Ice Age Paleoclimate

J.X. Mitrovica,[1] J. Austermann,[2] S. Coulson,[1] J.R. Creveling,[3] M.J. Hoggard,[1,2] G.T. Jarvis,[4] and F.D. Richards[5]

[1]Department of Earth and Planetary Sciences, Harvard University, Cambridge, Massachusetts 02138, USA; email: jxm@eps.harvard.edu

[2]Department of Earth and Environmental Sciences, Columbia University, Palisades, New York 10964-8000, USA

[3]College of Earth, Ocean and Atmospheric Sciences, Oregon State University, Corvallis, Oregon 97331, USA

[4]Department of Earth and Space Science and Engineering, York University, Toronto, Ontario M6E 3N1, Canada

[5]Department of Earth Science and Engineering, Imperial College London, London SW7 2AZ, United Kingdom

Annu. Rev. Earth Planet. Sci. 2020. 48:585–621

The *Annual Review of Earth and Planetary Sciences* is online at earth.annualreviews.org

https://doi.org/10.1146/annurev-earth-082517-010225

Keywords

dynamic topography, paleoclimate, sea level, ice age

Abstract

The connection between the geological record and dynamic topography driven by mantle convective flow has been established over widely varying temporal and spatial scales. As observations of the process have increased and numerical modeling of thermochemical convection has improved, a burgeoning direction of research targeting outstanding issues in ice age paleoclimate has emerged. This review focuses on studies of the Plio-Pleistocene ice age, including investigations of the stability of ice sheets during ice age warm periods and the inception of Northern Hemisphere glaciation. However, studies that have revealed nuanced connections of dynamic topography to biodiversity, ecology, ocean chemistry, and circulation since the start of the current ice-house world are also considered. In some cases, a recognition of the importance of dynamic topography resolves enigmatic events and in others it confounds already complex, unanswered questions. All such studies highlight the role of solid Earth geophysics in paleoclimate research and undermine a common assumption, beyond the field of glacial isostatic adjustment, that the solid Earth remains a rigid, passive substrate during the evolution of the ice age climate system.

- Dynamic topography is the large-scale, vertical deflection of Earth's crust driven by mantle convective flow.
- This review highlights recent research exploring the implications of the process on key issues in ice age paleoclimate.
- This research includes studies of ice sheet stability and inception as well as inferences of peak sea levels during periods of relative ice age warmth.
- This review also includes studies on longer timescales, continental-scale ecology and biodiversity, the long-term carbon cycle, and water flux across oceanic gateways.

1. INTRODUCTION

The theory of plate tectonics emerged from a unification of the complementary hypotheses of continental drift and seafloor spreading (e.g., Wilson 1965), and its development marked the dawn of modern global geophysics. Given this history, it is not surprising that the theory largely concerns horizontal movements on Earth's surface, at least in areas away from plate boundaries. Nevertheless, some of the earliest simulations of the driving force for plate tectonics—namely, thermochemical convection in Earth's mantle—demonstrated that such forces were also capable of driving long-wavelength, kilometer-scale vertical motions of Earth's surface (e.g., McKenzie et al. 1974). These vertical motions, supported by viscous stresses in the convective system, have come to be known as dynamic topography (e.g., Hager et al. 1985, Braun 2010, Flament et al. 2013).

The connection between dynamic topography and the geological record of epeirogeny was quickly established in the geophysical literature (e.g., Mitrovica et al. 1989; Gurnis 1990, 1992, 1993b). Mitrovica et al. (1989), following the original suggestion of Beaumont (1982), argued that viscous flow in the mantle coupled to subduction was capable of tilting overlying continents well beyond the location of foreland basins adjacent to mountain belts. They demonstrated, in particular, that long-wavelength, Cretaceous to Tertiary tilting of the Western Interior of North America was consistent with geologically inferred changes in the subduction history along the west coast of the continent (see also Lithgow-Bertelloni & Gurnis 1997). Similar arguments for subduction- (or subducted slab) controlled dynamic topography have been made to explain the stratigraphic record of the Russian Platform (Mitrovica et al. 1996), the Taranaki Basin of New Zealand (Holt & Stern 1994), the Australian continent (Gurnis et al. 1998, DiCaprio et al. 2009), the Karoo Basin of southern Africa (Pysklywec & Mitrovica 1999), the Baltic Basin (Daradich et al. 2002), northern South America (Shephard et al. 2010), and Southeast Asia (Zahirovic et al. 2016). Interactions between subducted slab material and the phase boundary at 670-km depth, which acts as a temporary impediment for flow into the lower mantle (Christensen & Yuen 1985), have also been identified as a mechanism for the development of transient intracontinental basins (Pysklywec & Mitrovica 1998)—for example, the Devonian to Carboniferous evolution of the Western Canada Sedimentary Basin (Pysklywec & Mitrovica 2000). In contrast to these regionally focused studies, Gurnis (1990, 1993b) was the first to recognize the global implications of subduction-driven inundation of continents, in particular on previous estimates of long-term global sea-level variations based on ridge spreading rates alone (Hayes & Pitman 1973).

Dynamic topography supported by rising mantle flow has also been associated with uplift of continental interiors, with African topography serving as a prime example. The large low-shear-velocity province below southern Africa (e.g., Ritsema et al. 2011) has been connected to anomalously high topography in this region (Hager et al. 1985, Lithgow-Bertelloni & Silver 1998, Gurnis et al. 2000, Jones et al. 2017), and the shallower, upper mantle continuation of the anomaly appears to be responsible for the present-day high topography of the East African Rift System

(Moucha & Forte 2011) and the tilt toward the northeast of the Arabian Plate (Daradich et al. 2003). Localized zones of upwelling mantle flow have also been associated with smaller-scale geological features, notably the uplift of the Colorado Plateau (Moucha et al. 2009), although the progressive removal of slab material may have also played a role in the event (Liu & Gurnis 2010).

Much recent numerical work has emphasized the global nature of dynamic topography (e.g., Zhang et al. 2012) and has returned to the issue of long-term sea-level changes (Moucha et al. 2008, Müller et al. 2008, Spasojevic et al. 2008, Conrad & Husson 2009, Spasojevic & Gurnis 2012, Conrad 2013, Flament et al. 2013, Cao et al. 2019). The important insight from these studies is that long-term, global-scale sea-level changes reflect the time-dependent, spatially integrated dynamic topography of ocean basins. However, these studies can disagree even on the sign of both regional and global sea-level change since the Cretaceous, and these conflicting estimates represent a key outstanding issue in global geophysical modeling of dynamic topography (Flament et al. 2013).

A broader, global-scale perspective on dynamic topography has also come from new observational constraints on the process. The regional studies listed above have generally relied on estimates of dynamic topography from preserved continental basin stratigraphy, or, in the case of the present day, from crustal corrections of raw topography to yield so-called residual topography. Each of these estimates is characterized by a number of error sources (Braun 2010) and relatively localized spatial extent. The latter limitation has been fundamentally improved by using compilations of seismic reflection data on continental shelves, largely collected by industry sources. Analyses of these data have, for example, connected estimates of dynamic topography with independently inferred Cenozoic vertical motions of the Indian peninsula (Richards et al. 2016) and Australia (Czarnota et al. 2013). Moreover, the power spectrum of present-day dynamic topography derived by Hoggard et al. (2016, 2017) from a global compilation of these seismic data sets is significantly discrepant from most previous numerical model predictions, raising a second key issue that is yet to be fully resolved (Yang & Gurnis 2016, Steinberger et al. 2017).

A number of excellent, comprehensive reviews of the physics, methodologies, and geological expressions of dynamic topography exist in the literature, and the interested reader is referred, for example, to Braun (2010), Flament et al. (2013), and Conrad (2013). In particular, Flament et al. (2013) describe and compare retrodictions based on three methods for reconstructing past variations in dynamic topography: subduction history modeling, backward advection, and adjoint modeling. Given this extensive literature, the present review focuses instead on a burgeoning new direction of research that is applying dynamic topography modeling to important, unresolved issues in ice age climate, with particular emphasis on the Plio-Pleistocene. Our focus on this time period reflects the availability of observational constraints and the limitations in retrodicting dynamic topography on longer timescales, but many of the results we discuss may hold important lessons for investigating ice-house climate events over the full span of Earth history (e.g., Creveling & Mitrovica 2014, Creveling et al. 2018, Pohl & Austermann 2018).

Earth's climate experienced a progressive cooling from the mid-Miocene to the Holocene and was subject to a series of critical climate events (Zachos et al. 2001). At the beginning of this period, ~14 Ma, permanent ice cover was established in the Antarctic, while the inception of Northern Hemisphere glaciation would not occur until the end of the so-called mid-Pliocene warm period (MPWP), at ~3 Ma (Zachos et al. 2001). Over this span of time, oxygen isotope records, as well as a variety of other climate proxies, record Milankovitch cyclicity in ocean temperatures and continental ice volume (e.g., Lisiecki & Raymo 2005). In the period prior to the MPWP, the cycles had muted amplitude, suggesting relatively moderate, obliquity-forced fluctuations in Antarctic ice volume. After the MPWP, the amplitudes increased significantly as Earth's climate cooled and grounded ice sheets took hold in the Northern Hemisphere, including North America, Greenland, and Eurasia.

At 0.8 Ma, the enigmatic mid-Pleistocene transition occurred as the obliquity-dominated (41-kyr period) climate signal was replaced by cycles of period 100 kyr (Raymo et al. 1997, Clark & Pollard 1998, Huybers 2006). Each of these cycles was characterized by a relatively slow glaciation phase and a more rapid deglaciation followed by an interglacial period of variable duration (Lisiecki & Raymo 2005). However, as proxy records of increasingly refined temporal resolution became available—in particular, ice cores with their annual lamina still distinct—the traditional, so-called textbook view of a simple saw-tooth fluctuation in ice volumes has given way to a recognition of dramatic, millennial-scale variability in climate (e.g., Dansgaard-Oeschger and Heinrich events) across glacial cycles (Dansgaard et al. 1982, Andersen et al. 2004).

While this broad picture of recent ice age climate has come into focus, a number of seminal questions remain unanswered. For example, how stable was the Antarctic Ice Sheet (AIS) during the MPWP, and how high did global mean sea level (GMSL) reach during the so-called superinterglacials (Raymo et al. 2011; Miller et al. 2012; Rowley et al. 2013; Rovere et al. 2014, 2015)? What sequence of events triggered glacial inception in the Northern Hemisphere, and why did permanent ice cover apparently first take hold on Baffin Island (Hall & King 1989) and possibly Greenland (Steinberger et al. 2015)? What was peak GMSL during the Last Interglacial (LIG), that is, Marine Isotope Stage (MIS) 5e, at ∼120 ka (Kopp et al. 2009, Dutton & Lambeck 2012), or during the longest duration interglacial of the past 800 kyr, MIS 11, at ∼420 ka (Raymo & Mitrovica 2012)? Furthermore, how did melting from the Greenland Ice Sheet (GIS), West Antarctic Ice Sheet (WAIS), and East Antarctic Ice Sheet (EAIS) contribute to the peak GMSL? The last of these issues, the inference of individual meltwater sources, is a key motivation in efforts to move beyond estimates of peak GMSL to constrain the geographic variability of sea-level changes (Mitrovica et al. 2001).

Most of the above questions are motivated by a desire to elucidate the stability of ice sheets during periods of relative ice age warmth and to use the answers to gain insight into polar ice sheet stability in our progressively warming world. In this review, we make the case that over the timescales relevant to each of the above issues, dynamic topography of the solid Earth plays an important role and must be considered. In some cases, this requirement confounds already complex problems, but in others, it resolves enigmatic observations that have been interpreted under an assumption, explicit or not, that the solid Earth is a rigid, passive substrate during the evolution of Earth's climate system.

The calculations summarized below are largely based on convection simulations using the ASPECT (Advanced Solver for Problems in Earth's ConvecTion) code that solves the coupled equations governing conservation of mass, momentum, and energy in a compressible, momentum-free mantle (Kronbichler et al. 2012, Bangerth et al. 2014, Heister et al. 2017). Mantle convective flow is driven by buoyancy (lateral density) variations, which in the ASPECT-based simulations are inferred from a mapping between perturbations in seismic velocity and density and are resisted by the viscosity of mantle material. The seismic velocity-to-density mapping and viscosity are generally tuned, either together or separately, to fit to some set of observations related to convection or glacial isostatic adjustment (GIA) or both. Time-dependent dynamic topography, $h(t)$, is computed in the simulations from the following relation (e.g., Flament et al. 2013):

$$\sigma_{rr}(t) = \Delta\rho g h(t) \qquad 1.$$

as

$$h(t) = \sigma_{rr}(t)/(\Delta\rho g), \qquad 2.$$

where σ_{rr} is the normal stress computed at the surface of the convection cell (which is constrained for numerical reasons to remain a level surface), $\Delta\rho$ is the density jump at the surface (i.e., from mantle to either air or water), and g is the gravitational acceleration. Normal stresses, and hence dynamic topography, always arise at the upper surface when lateral temperature gradients are present in the shallow mantle. To compute dynamic topography over time at a given site requires that the signal from Equation 2 be augmented to track plate motions relative to the underlying mantle. Equation 2 is generally solved by adopting fixed values of $\Delta\rho$; however, Austermann & Mitrovica (2015) have described a methodology for computing sea-level changes due to dynamic topography that accounts for water loading in the case of migrating shorelines (i.e., a switch from water to air cover, or vice versa, at a given site) and flexure of an elastic lithosphere. For details of each calculation of dynamic topography described below, we refer readers to the primary citations listed in each section.

As a final point, there has been a long-standing debate within the geophysical literature of dynamic topography as to whether the term dynamic topography should include subsidence of the oceanic lithosphere as it moves away from the ridge and cools (Forte et al. 1993, Gurnis 1993a). The distinction is a semantic one as long as comparisons between observations and predictions adopt a consistent definition. In any event, unless otherwise stated, the calculations of dynamic topography presented in this review include the signal associated with cooling of the oceanic lithosphere since they are based on results from simulations of mantle convection.

2. MID-PLIOCENE SEA-LEVEL AND ICE SHEET STABILITY

The MPWP (3.3–3.0 Ma) marks the last time in Earth history that atmospheric CO_2 levels reached ~400 ppm (Pagani et al. 2010). A variety of climate proxy data and general circulation modeling results suggest that global mean sea surface temperatures and surface air temperatures during the MPWP were at least 2°C higher than preindustrial values (Lunt et al. 2010, Haywood et al. 2013, Dowsett et al. 2016). In contrast to this consensus, there is significantly less agreement on the peak GMSL rise attained during the interglacials of the MPWP. Indeed, a summary statement within the Fifth Assessment Report of the Intergovernmental Panel for Climate Change reads, "there is *high confidence* that GMSL was above present, due to deglaciation of GIS, WAIS and areas of EAIS, and that sea level was not higher than 20 m above present during the interglacials of the MPWP" (Masson-Delmotte et al. 2013). The importance of reducing this uncertainty cannot be overstated. A value at the higher end of this range would not only require collapse of the GIS and WAIS but also indicate significant ice mass loss from the EAIS, which is traditionally seen as the more stable component of the cryosphere-climate system (Masson-Delmotte et al. 2013). Estimates of peak GMSL during the MPWP have been based on ice sheet and climate modeling, isotopic analyses of ocean sedimentary cores, and mapping of paleoshoreline deposits. Each of these approaches has limitations, which we describe in turn.

Numerical simulations of ice sheet stability using climatic conditions consistent with MPWP suggest melt from the GIS (+7 m equivalent GMSL), WAIS (+4 m), and margins of marine-based sectors of the EAIS (+3 m) totaling 14 m or less (Lunt et al. 2008, Pollard & DeConto 2009, Masson-Delmotte et al. 2013, de Boer et al. 2015). It has been argued that the Antarctic contribution to the above total could be increased by as much as 10 m by including hydrofracturing from surface melt and ice cliff failure in ice sheet modeling (Pollard et al. 2015), but recent modeling has raised doubt about this conclusion (Edwards et al. 2019). In addition, the above estimates of marine-based ice loss did not incorporate the stabilizing effect on melting ice sheets of sea-level fall at the grounding line (e.g., Gomez et al. 2010, 2018).

Estimates of peak GMSL during the MPWP have been derived by scaling of benthic oxygen isotope ($\delta^{18}O$) anomalies collected from ocean sediment cores (e.g., Miller et al. 2005), but interpreting these records is complicated by entangled sensitivities to temperature, regional hydrography, meltwater source distribution, and other factors (Masson-Delmotte et al. 2013, Raymo et al. 2018). Additional data sets have been used to augment the $\delta^{18}O$ data, including Mg/Ca ratios (which have a temperature dependence related to the calcification process), and seismic stratigraphic analysis on continental margin sites and atolls, but these data sets have their own limitations (Miller et al. 2012), and estimates based upon them continue to vary by tens of meters (Dwyer & Chandler 2009, Naish & Wilson 2009, Sosdian & Rosenthal 2009, Miller et al. 2012).

Field mapping of paleoshorelines represents a third major approach to constraining peak sea level during the MPWP. Studies of this type have considered mid-Pliocene shoreline records on the Roe Plain on the western portion of the Great Australian Bight (~30 m) (James et al. 2006), the Nome coastal plain of Alaska (60 m) (Kaufman & Brigham-Grette 1993), the Enewetak Atoll in the western Pacific (20–25 m) (Wardlaw & Quinn 1991), the Moorhouse Formation in Virginia (15–20 m) (Krantz 1991), and the Orangeburg Scarp extending ~1,000 km along the coastal plain of the eastern United States (35 m) (Dowsett & Cronin 1990). Raymo et al. (2011) modeled the potential contamination of these estimates by the signal associated with GIA and was the first to suggest that corrections for local sediment loading and dynamic topography may be an important source of error in previous estimates of peak GMSL based on paleoshoreline heights. We discuss these corrections in the next section, with a focus on the Orangeburg Scarp and the study of Rowley et al. (2013).

2.1. Dynamic Topography and the Present-Day Elevation of the Orangeburg Scarp

Preserved remnants of a mid-Pliocene shoreline along the Atlantic coastal plain of the United States extend from Virginia to Georgia (e.g., Winker & Howard 1977) (**Figure 1*a***). We refer below to the entire paleoshoreline as the Orangeburg Scarp, although it is also known as the Chippenham Scarp and Thornburg Scarp in southern and northern Virginia, respectively. Because of its length, the Orangeburg Scarp has served as a major focus in efforts to constrain GMSL during the MPWP (Dowsett & Cronin 1990; Raymo et al. 2011; Rowley et al. 2013; Rovere et al. 2014, 2015). Recently, Rovere et al. (2015) combined geological maps, geomorphic analyses, and satellite data with new field measurements based on surveying using the Global Positioning System and digital elevation models to derive a more robust elevation database for the scarp. Their profile is shown on **Figure 2**. The scarp is characterized by a general increase in elevation from ~35 m at the border of Georgia and South Carolina (32°N) to 85 m on the central coast of North Carolina (35°N). It then decreases relatively sharply to 60 m over a distance of ~90 km and then gradually increases northward to reach 80 m on the central coast of Virginia (38°N).

The variable elevation of the scarp indicates significant postdepositional deformation of the paleoshoreline. Dowsett & Cronin (1990) adopted the Winker & Howard (1977) value for the elevation of the Orangeburg Scarp at a site close to the border between North and South Carolina (85 m), and they corrected this elevation using both the mean and peak uplift rates determined from river terraces near the Cape Fear Arch (Soller 1989) to estimate sea-level highstands of 53 ± 9 m and 17 ± 9 m, respectively. They combined these to arrive at their final estimate of 35 ± 18 m, which they interpreted as a golden sea-level spike—that is, an uncontaminated estimate of peak GMSL during the MPWP. Dowsett & Cronin (1990) further argued that the lower elevation of the Orangeburg Scarp in Georgia (32°N) (**Figure 2**) suggests tectonic stability in this region.

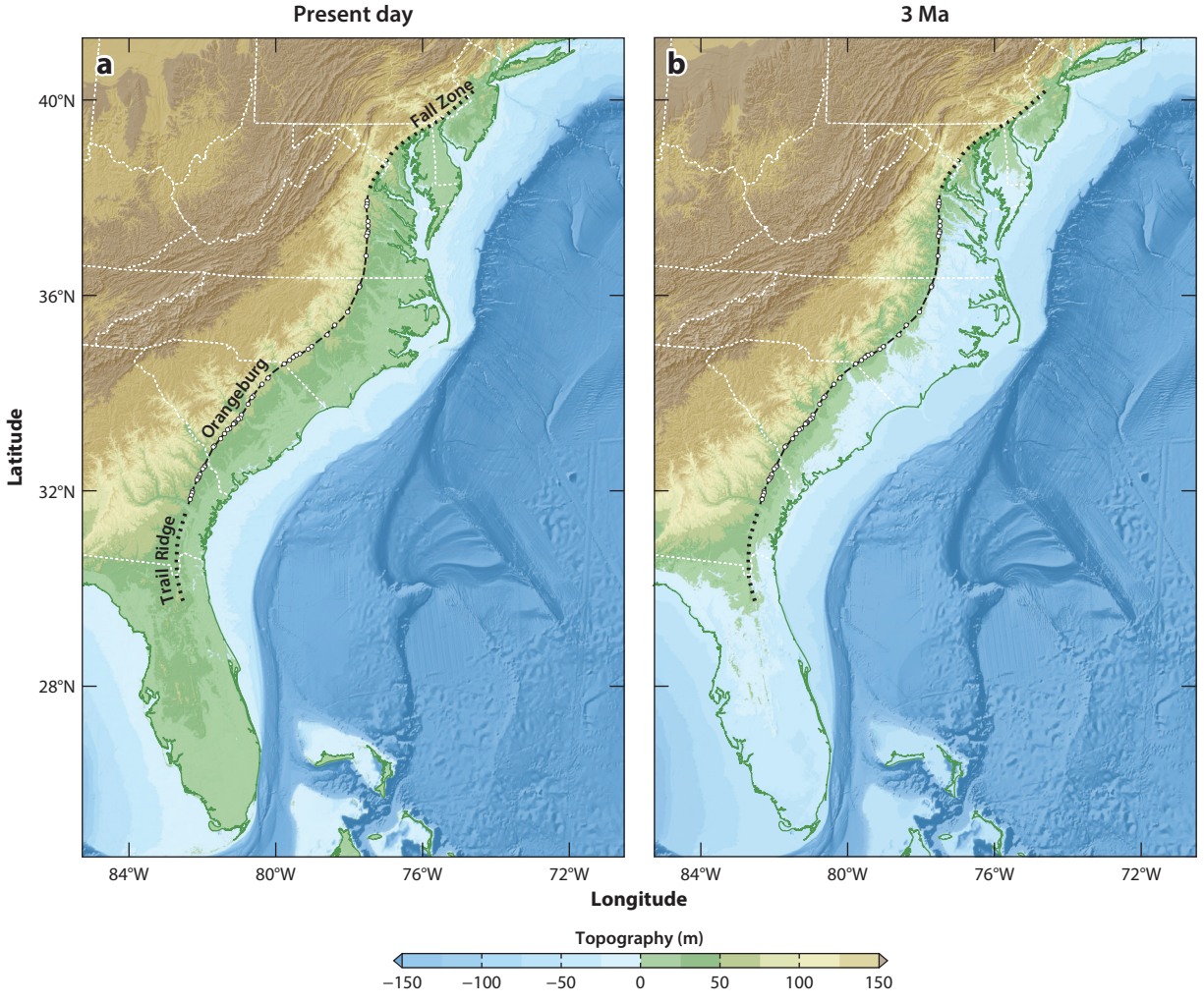

Figure 1

(*a*) Present-day topography along the Atlantic coastal plain of the United States, with the location of the Orangeburg Scarp, Trail Ridge, and Fall Zone superimposed. White circles indicate locations with the most accurate elevation measurements (Rovere et al. 2015). (*b*) Paleotopography at 3 Ma was reconstructed by applying corrections for both glacial isostatic adjustment and dynamic topography. Both corrections were generated using simulations that adopt the V2 mantle viscosity profile (Mitrovica & Forte 2004, Moucha et al. 2008, Rowley et al. 2013). The dynamic topography calculation adopts the TX2007 density field (Simmons et al. 2007).

Raymo et al. (2011) recognized that most of the Atlantic coastal plain lies within the peripheral zone of the Laurentide Ice Sheet that covered most of Canada and the northeastern United States at the Last Glacial Maximum (Clark et al. 2009), and thus it was subject to significant vertical deflection from GIA. During the glacial phase, the periphery bulges upward and sea level falls, while during the deglacial and interglacial phases, the bulge subsides, and sea level rises toward its original (unloaded) state. The present isostatic disequilibrium along the coastal plain is sensitive to only the last glacial cycle since adjustments in response to previous cycles will be complete. Hence, a shoreline that formed within the peripheral bulge of the Laurentide Ice Sheet during the mid-Pliocene will lie above present-day sea level, and, as peripheral bulge subsidence (isostatic

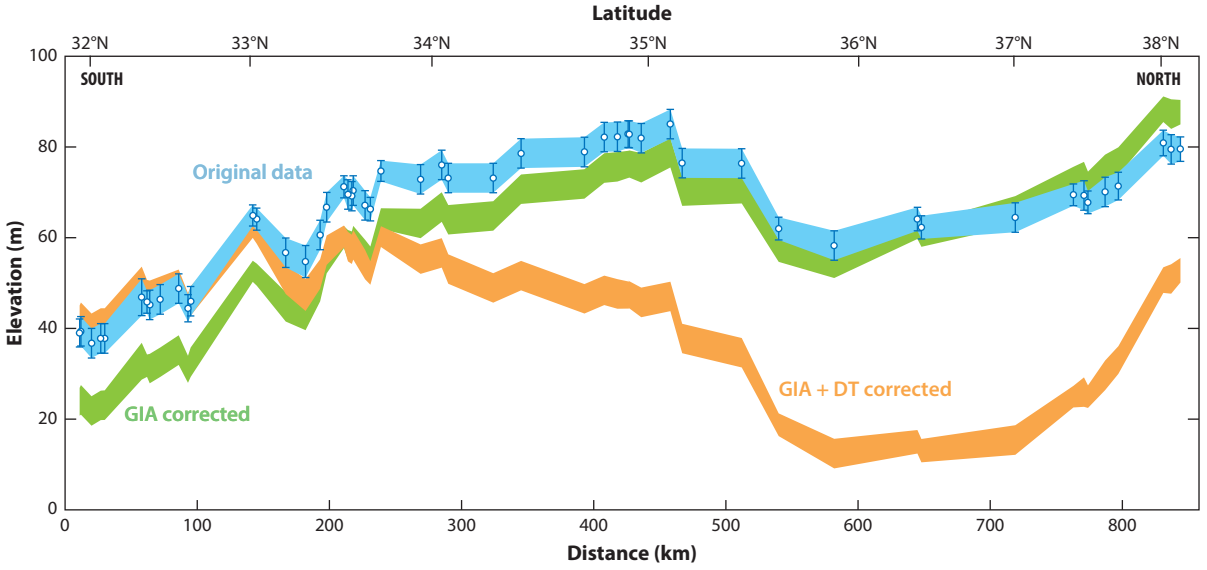

Figure 2

Blue is the elevation northward along the Orangeburg Scarp (adapted from Rovere et al. 2015). Green is the elevation after correction for glacial isostatic adjustment (GIA); orange is after correction for both GIA and dynamic topography (DT). Both corrections were generated using simulations that adopt the V2 mantle viscosity profile (Mitrovica & Forte 2004, Moucha et al. 2008, Rowley et al. 2013). The DT calculation adopts the TX2007 density field (Simmons et al. 2007).

adjustment) continues to drive sea-level rise, the elevation of the paleoshoreline will progressively fall.

Figure 3*a* shows a prediction of the remnant deflection of any locality along the Atlantic coastal plain of the United States due to incomplete GIA in response to the glacial cycles extending over the past 3 Myr. The full details of the calculation are found in Raymo et al. (2011). The only difference with the results appearing in that earlier paper (e.g., their figures 2*C* and 3*C*) is that the simulation in **Figure 3*a*** is based on the V2 viscosity model generated by joint inversion of a suite of data related to both GIA and mantle convection (Mitrovica & Forte 2004, Moucha et al. 2008, Rowley et al. 2013; see also Rovere et al. 2015). The V2 model is characterized by a three order of magnitude increase in viscosity from the base of the lithosphere (10^{20} Pa s) to a mid-lower mantle depth of 2,000 km (10^{23} Pa s), followed by a decrease in viscosity back to a value close to 10^{20} Pa s above the core-mantle boundary. Moving north to south along the scarp, the ice age signal increases from −6 to +14 m. **Figure 2** shows the impact of correcting the present-day elevation of the Orangeburg Scarp for this ice age deformation. GIA does not explain the variability in the present-day elevation of the scarp (Rovere et al. 2015). The question arises: Can dynamic topography account for the remnant signal in the elevation of the scarp and its location within the interior of the continent?

Rowley et al. (2013) presented four different predictions of dynamic topography change since 3 Ma computed using the backward-advection procedure described by Moucha et al. (2008), following Forte & Mitrovica (1997), in which time is reversed in the equations governing mantle convection and diffusion is set to zero in the heat equation. The four simulations were generated using two different radial viscosity profiles, the V2 profile discussed above and a variant on this profile characterized by a thin, low-viscosity ($\sim 5 \times 10^{19}$ Pa s) layer at the base of the upper mantle (V1), and two different inferences of the three-dimensional (3D) mantle density field, TX2007

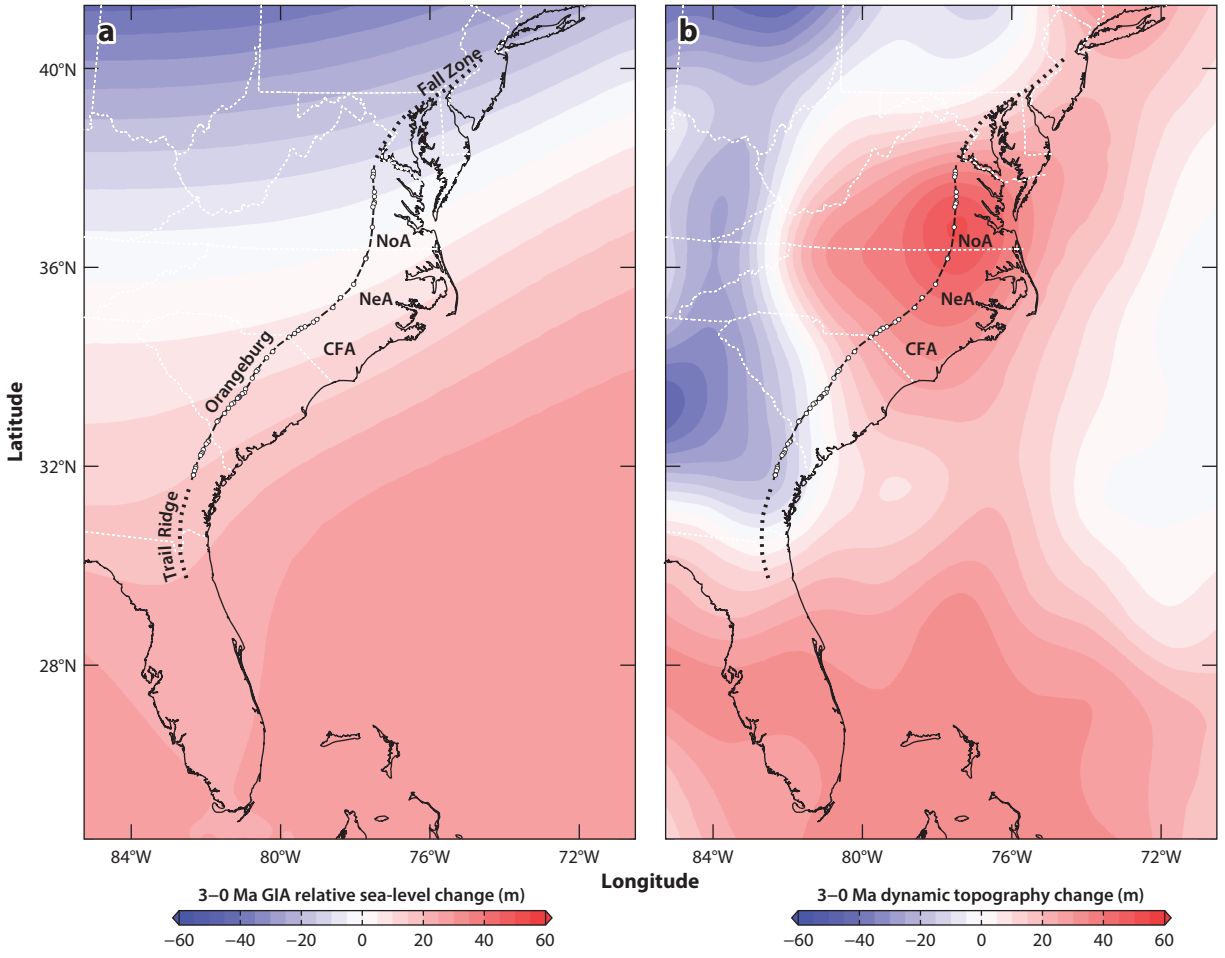

Figure 3

(*a*) Numerical simulation of relative sea level at 3 Ma within the Atlantic coastal plain of the United States associated with the GIA process assuming no change in global mean sea level (i.e., ice volumes) after 3 Ma. (*b*) Change in elevation associated with dynamic topography. Both calculations adopt the V2 mantle viscosity profile, and the dynamic topography prediction is based on the TX2007 density field (Simmons et al. 2007, Rowley et al. 2013). The green line in **Figure 2** was computed by correcting the raw elevation along the Orangeburg Scarp for the prediction in panel *a*, while the orange line in **Figure 2** added an additional correction for dynamic topography shown in panel *b*. Abbreviations: CFA, Cape Fear Arch; GIA, glacial isostatic adjustment; NeA, Neuse Arch; NoA, Norfolk Arch.

(Simmons et al. 2007) and TX2008 (Simmons et al. 2009). Rovere et al. (2015) noted that the dynamic topography prediction associated with the combination of the V2 viscosity model and the TX2007 density field most accurately predicted the residual (post-GIA correction) elevation of the Orangeburg Scarp shown in **Figure 2**, and we focus on that pairing here. The TX2007 density field was generated from a simultaneous inversion of a global seismic data set (approximately 46,000 shear-wave travel-time observations) and a suite of convection-related surface observations, including free air gravity anomalies, plate motions, dynamic topography, and the excess ellipticity of the core-mantle boundary inferred from free-core nutation observations (Simmons et al. 2007). For internal consistency, the inversion adopted a viscosity model within the class of

models generated by Mitrovica & Forte (2004) in their simultaneous inversion of convection and GIA data sets.

The change in dynamic topography computed using the V2-TX2007 pairing is shown in **Figure 3*b*** (Rowley et al. 2013). As noted by Rowley et al. (2013), the variability in the field along the Atlantic coastal plain is qualitatively consistent with several regional geological features. For example, the zone of significant predicted dynamic uplift in the northern section of the scarp coincides with the Norfolk Arch in Virginia, the Neuse Arch in North Carolina, and the Cape Fear Arch near the border of the Carolinas.

In **Figure 2** we show the impact of correcting the elevation of the Orangeburg Scarp for both the GIA and dynamic topography fields of **Figure 3*a*** and ***b***, respectively, while **Figure 1*b*** reconstructs topography and shoreline location at 3 Ma generated from this topography. The correction for GIA and dynamic topography yields an accurate reconstruction of the geographic location of the Orangeburg Scarp northward of 35°N to the start of the Fall Zone but a systematic misfit south of 35°N (**Figure 1**; see also Rowley et al. 2013). This misfit pattern may reflect, to some extent, the higher gradient in topography on the coastal plain (i.e., oceanward of the scarp) south of the Cape Fear Arch relative to the north, which would accentuate misfits in the reconstructed position of the shoreline at these lower latitudes.

There have been suggestions that crustal deformation associated with variable sediment redistribution along the coastal plain may be responsible for the misfit between the reconstructed position of the 3 Ma shoreline in **Figure 1*b*** and the location of the Orangeburg Scarp and the along-strike variation in the residual elevation of the scarp (i.e., after correction for GIA and dynamic topography) (**Figure 2**). Moucha & Reutenik (2017) varied parameters in a landscape evolution model and argued that the residual signal was well fit by a combination of simple elastic flexure due to sediment redistribution and a GMSL rise of 15 m during the MPWP. Q. Li, K.L. Ferrier, J. Austermann, & J.X. Mitrovica (unpublished article) combined a new database of erosion and deposition rates in the region with an ice age sea-level calculator (Pico et al. 2016, Ferrier et al. 2017) to retrodict sea-level changes within the coastal plain and argued that an uplift signal from sediment redistribution could reach ∼20 m along the Orangeburg Scarp, with relatively strong gradients in the vicinity of the Cape Fear Arch.

The sharp gradient in the raw elevation profile and the GIA-corrected profile at ∼35.0–35.5°N, just north of the Cape Fear Arch (**Figure 2**), has also led to speculation that there may have been displacement since 3 Ma across a fault system inferred by Marple & Talwani (2000) on the basis of a broad suite of geological and geophysical evidence (Rovere et al. 2015). However, this feature appears to be part of a broader-scale undulation in the elevation profile after the additional correction for dynamic topography (**Figure 2**). The residual elevation in this case, which is characterized by a peak-to-peak amplitude of ∼50 m, is more suggestive of an error in the dynamic topography correction (**Figure 3*b***).

Clearly, further work is necessary to robustly isolate GMSL (or, equivalently, ice volumes) at 3 Ma from the various physical processes contributing to the present-day elevation of the Orangeburg Scarp. Reducing uncertainty in the dynamic topography signal should remain a key target in this regard. Indeed, while Rowley et al. (2013), following Moucha et al. (2008), predict a dynamic uplift of the Atlantic coastal plain since 3 Ma, Müller et al. (2008), Spasojevic et al. (2008), and Conrad & Husson (2009) predict subsidence over this period. Seismic tomography indicates that the mantle below the coastal plain is characterized by a descending Farallon slab that extends to mid-mantle depth and a shallower zone of low seismic velocity to the east of the slab, suggestive of hot, upwelling material (Simmons et al. 2009). In the Moucha et al. (2008) simulations, this combination of forcing yields a dynamic tilting toward the west of the crust (i.e., uplift of the coastal plain). In contrast, the subsidence predicted in the modeling of Müller et al. (2008),

Spasojevic et al. (2008), and Conrad & Husson (2009) is a result of a dominance of the Farallon slab in controlling mantle flow beneath the scarp in their simulations.

Flament et al. (2013) suggested that the difference in the sign of the dynamic topography predictions may be due to the viscosity profile adopted by Rowley et al. (2013) and Moucha et al. (2008), which included a low-viscosity notch at the base of the upper mantle that would act to decouple lower mantle flow from the shallow mantle and thus diminish the influence of the Farallon slab on surface topography. However, uplift of the coastal plain in **Figure 3*b*** is based on a model (V2) with essentially no low-viscosity notch at the base of the upper mantle. It is more likely that the difference in the sign of the dynamic topography prediction arises from the treatment of the shallow zone of low seismic velocity and the conversion of this velocity anomaly into a buoyancy field in the various studies. In any case, the GIA-corrected profile in **Figure 2** argues against dynamic subsidence of the coastal plain since the MPWP. A prediction of subsidence implies an upward correction of this profile to account for dynamic topography, and even in the case of a 20-m sediment loading correction, the peak residual elevation, if associated with a change in GMSL, would imply full deglaciation of all ice masses now extant on Earth's surface during the MPWP.

2.2. How Dynamic Was the East Antarctic Ice Sheet During the Mid-Pliocene Warm Period?

The ongoing uncertainty associated with peak GMSL during the MPWP has been compounded by conflicting geological evidence related to the Pliocene stability of the EAIS. Field data from the Dry Valleys on the eastern margin of the Ross Sea (**Figure 4**), including well-dated ash deposits, suggest that the EAIS has been cold based and stable since the early Miocene (Denton et al. 1993). In contrast, glacial deposits in the Dominion Range of the Transantarctic Mountains include marine diatoms of Pliocene age and have been interpreted as reworked sediments from sectors of the East Antarctic that were ice free into the late Pliocene (Webb et al. 1984). This argument requires either (*a*) that the sediments were deposited by ice flow up the Transantarctic Mountains or (*b*) rapid uplift of the Dominion Range (**Figure 4**) of order 600 m/Myr. The latter is inconsistent with surface exposure dating and geomorphological analyses that suggest that the area has uplifted by less than a few hundred meters since the MPWP and that it has remained within a cold, arid climate (Ackert & Kurtz 2004). Moreover, an earlier advance of a warm-based EAIS across the Transantarctic Mountains may have deposited the glacial sediments on the Dominion Range (Mayewski & Goldthwait 1985), and it has also been conjectured that the marine diatoms may have been windblown from a much lower elevation (Stroeven et al. 1996, Scherer et al. 2016). Geological evidence for a dynamic EAIS during the MPWP is not, however, limited to the Dominion Range. Stratigraphic and sedimentological data indicate that the Lambert Glacier, which currently terminates in Prydz Bay (**Figure 4**), experienced major episodes of advance and retreat into the Late Pleistocene (Hambrey & McKelvey 2000). In addition, a recent geochemical provenance study of detrital material on the Antarctic margin suggests significant Pliocene retreat of the EAIS from the Wilkes Subglacial Basin (Cook et al. 2013) (**Figure 4**).

These various lines of evidence, and the contentious debate surrounding them (Ackert & Kurtz 2004), motivate the question that provides the title of this section: How dynamic was the EAIS during the MPWP? As noted earlier, ice sheet modeling based on mid-Pliocene climate indicates a peak GMSL of less than 14 m derived mainly from the GIS and WAIS (Lunt et al. 2008, Pollard & DeConto 2009, de Boer et al. 2015, Masson-Delmotte et al. 2013). How can this be reconciled with the robust data from Prydz Bay (Hambrey & McKelvey 2000) and the Wilkes Basin (Cook et al. 2013) that suggest at least local instability of the EAIS? An important limitation of previous ice sheet models is their method of reconstructing ancient bedrock topography. These

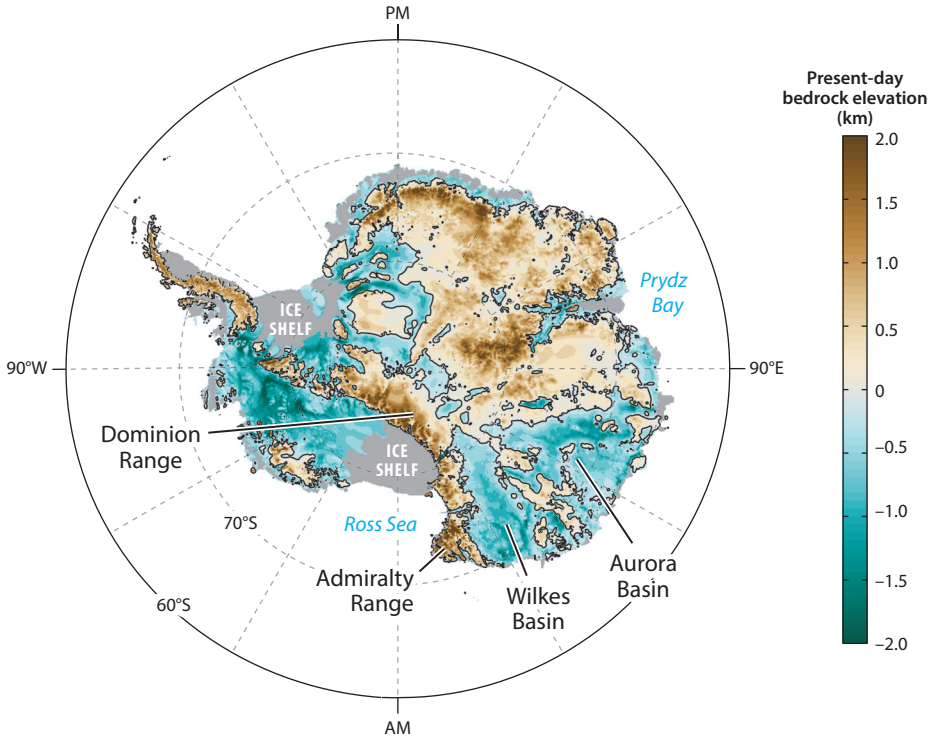

Figure 4

Present-day bedrock elevation across Antarctica from Bedmap2 (Fretwell et al. 2013) showing the location of sites mentioned in the main text. Figure adapted from Austermann et al. (2015).

reconstructions are generally based on a simple isostatic correction to present-day bedrock topography to account for the difference in ice thickness between the time of interest and the modern day. Recent studies using coupled ice sheet/sea-level modeling (Gomez et al. 2010, 2013, 2018) have demonstrated that the incorporation of gravitationally self-consistent postglacial sea-level (or, equivalently, topography) changes can, for example, have a significant impact on the predicted evolution of the AIS since the Last Glacial Maximum. In the case of the MPWP, any reconstruction of bedrock topography should also consider a correction for the change in dynamic topography over the past 3 Myr (Austermann et al. 2015), as well as erosion and tectonic effects (Paxman 2019).

The bedrock topography map of the Antarctic shows significant marine-based regions—that is, areas where crustal elevations lie below the local sea surface equipotential (**Figure 4**). When these regions are characterized by reverse bed slopes (i.e., bedrock elevation decreases toward the center of the ice sheet), any overlying, grounded ice complexes are susceptible to a runaway instability mechanism that has come to be known as the marine ice sheet instability hypothesis (Weertman 1974). Simply put, a grounded marine ice sheet gains mass from precipitation and loses mass via gravitationally driven horizontal mass flux across the grounding line (the line that marks the transition from a grounded ice sheet to a floating ice shelf). When an ice sheet grounded on a reverse bed slope melts back, the horizontal mass flux across the grounding line increases, leading to further retreat of the grounding line and a further increase in the mass loss. In this canonical picture, the process will continue until the bed slope changes sign. The West Antarctic is largely characterized by a marine-based setting and reverse bed slopes (**Figure 4**), and this is

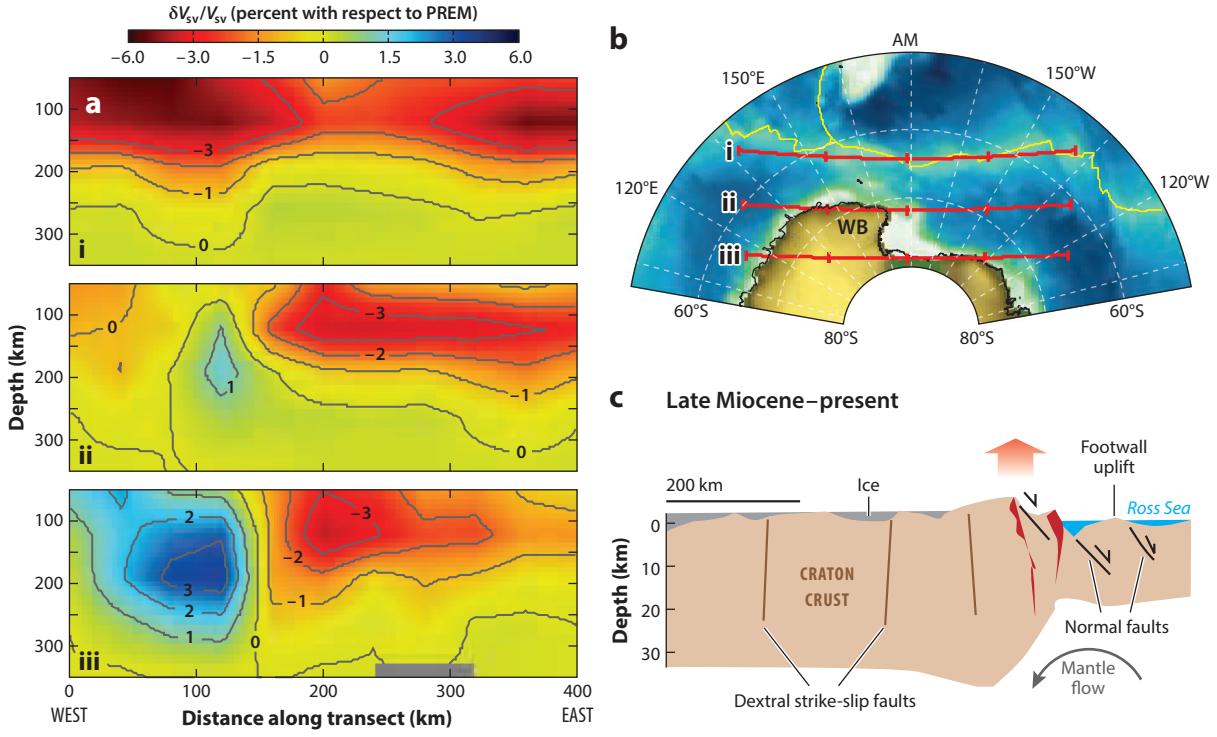

Figure 5

(*a*) Relative perturbations in shear-wave velocity to a depth of 350 km on the three vertical cross sections shown in panel *b*. (*c*) Schematic illustration of crustal deformation, uplift, and mantle flow below the Ross Sea–Transantarctic Mountain region. Abbreviations: PREM, Preliminary Reference Earth Model; WB, Wilkes Basin. Figure adapted from Faccenna et al. (2008).

the reason WAIS is considered particularly susceptible to collapse in a warming world. However, **Figure 4** also shows that large areas of the EAIS are marine based at present and grounded on reverse bed slopes (e.g., the Wilkes and Aurora Basins and Prydz Bay). A collapse of the EAIS in these sectors would lead to 14 m of GMSL rise, compared to 3.5 m if all grounded, marine-based ice within WAIS disappeared.

Spasojevic et al. (2010) combined a wide range of models and observations (seismic tomography, topography, gravity, plate reconstructions) with a time-evolving, global model of mantle dynamics to explore the evolution of mantle flow and plate tectonics in the Antarctic-New Zealand region since the Late Cretaceous. They noted that a low-velocity anomaly in the shallow mantle—extending from New Zealand to the Ross Sea and Marie Byrd Land in the West Antarctic—is a consistent feature of a number of published seismic models, and their flow calculations predict uplift of the Ross Sea, the Admiralty Mountains, and parts of the Wilkes Basin since at least 20 Ma (see Spasojevic et al. 2010, figure 6*A*). Faccenna et al. (2008) presented mantle flow models focused on the Ross Sea and Admiralty Mountain region. **Figure 5**, adapted from their study, shows seismic velocity anomalies in three vertical cross sections moving southward across the region. Profiles II and III in **Figure 5*a*** are characterized by a shallow velocity anomaly beneath the Ross Sea impinging on the thick lithospheric root of the East Antarctic Craton. The associated flow models, summarized by the schematic in **Figure 5*c***, predict crustal extension across the region that is consistent with the geological record of faulting and volcanism and a

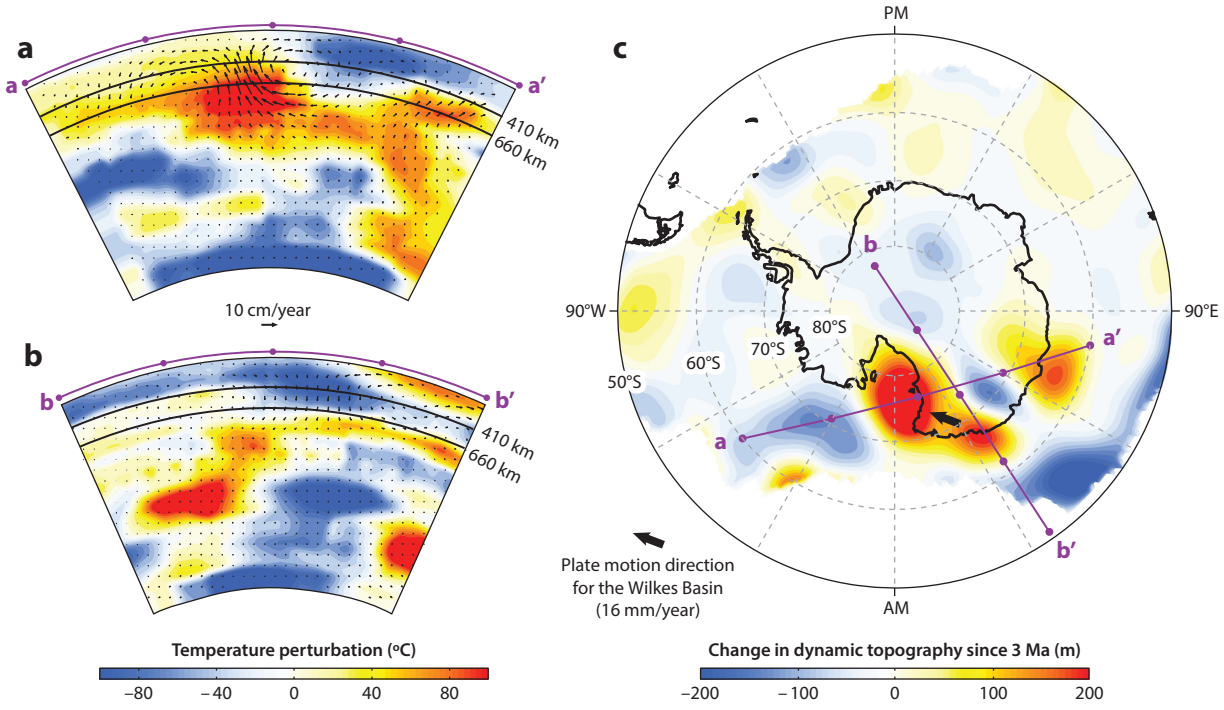

Figure 6

(*a*,*b*) Present-day temperature perturbations and flow velocities inferred from a mantle convection simulation within two vertical cross sections through the Wilkes Basin. The orientation of the profiles is shown in panel *c*. (*c*) Dynamic topography change over the past 3 Ma predicted by backward advection of the flow fields in panels *a* and *b*. Figure adapted from Austermann et al. (2015).

recent phase of uplift of the Admiralty Mountains driven by small-scale convection associated with the low seismic velocity anomaly in the lower two panels of **Figure 5*a***.

The analysis of Faccenna et al. (2008) is supported by Austermann et al. (2015), who performed a backward-advection calculation of mantle flow to track dynamic tomography in the Antarctic over the past 3 Ma. Their simulation is based on the V2 viscosity model (Mitrovica & Forte 2004) adopted in the results of **Figures 1–3** and the mantle density model TX2008 (Simmons et al. 2009). **Figure 6*a*** and ***b*** show snapshots of present-day mantle temperature and flow velocities in two vertical cross sections through the East Antarctic (the intersection of these profiles occurs in the Wilkes Basin). The orientation of cross section aa′ is approximately the same as the profiles II and III in **Figure 5*a***, and, as in the Faccenna et al. (2008) study, it reveals the presence of high-temperature, thermally buoyant material in the shallow mantle below the Ross Sea and Transantarctic Mountains that extends to meet the root of the East Antarctic Craton. A prediction of dynamic topography change over the past 3 Myr associated with this flow field that also accounts for horizontal motion of the Antarctic relative to the underlying mantle (Sella et al. 2002) is shown in **Figure 6*c***. The upwelling in the flow simulation drives an uplift field of peak magnitude ∼250 m that extends from the Ross Sea, across the Dry Valleys sector of the Transantarctic Mountains, and into the Wilkes Basin. This prediction is consistent with an upper bound on uplift of this sector (<300 m) derived via mapping and geochronology of cinder cone deposits (Wilch et al. 1993). Other regions of the Antarctic are predicted to have experienced significantly less change in dynamic topography (**Figure 6*c***).

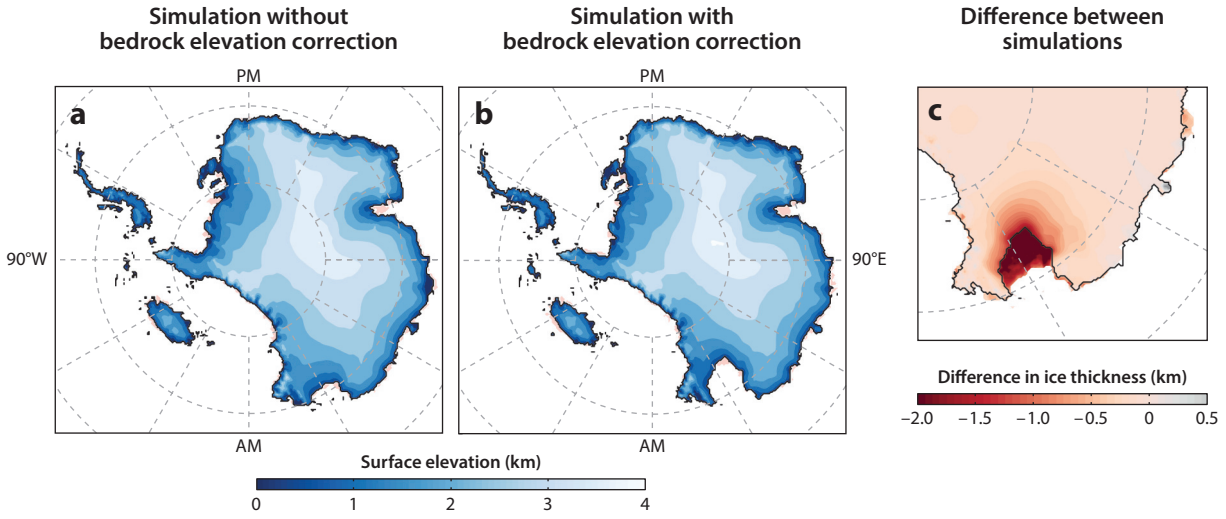

Figure 7

(*a*,*b*) Simulations of ice sheet surface elevation over the Antarctic during the mid-Pliocene warm period. The result in panel *a* is based on a simulation where no correction is made for dynamic topography change to establish mid-Pliocene bedrock elevation. In contrast, the result in panel *b* corrects bedrock elevation using the prediction of dynamic topography change in **Figure 6*c***. (*c*) The difference in ice thickness predicted in the two simulations (i.e., prediction with the dynamic topography correction minus prediction without). Figure adapted from Austermann et al. (2015).

The simulation in **Figure 6*c*** thus suggests that the bedrock in this region at 3 Ma may have been hundreds of meters lower than the present-day bedrock elevation. To explore the implications of this inference for EAIS stability, Austermann et al. (2015) used the reconstructed topography as input to an ice sheet model. Specifically, they used the model of Pollard & DeConto (2009) and DeConto et al. (2012) forced with conditions appropriate to the Pliocene (Pollard et al. 2015), including the adoption of independent reconstructions of atmospheric temperatures and CO_2 concentration (400 ppm), surface ocean warming of 2°C relative to present day, and obliquity-dominated changes in summer solar insolation. Results of ice sheet simulations in which the mid-Pliocene bedrock topography is not—or, alternately, is—corrected for the change in dynamic topography are shown in **Figure 7*a*** and ***b***, respectively. Both simulations predict full collapse of marine-based sectors of WAIS. The primary disparity between the two results occurs in the Wilkes Basin, as reflected in the map of the predicted difference in ice thickness (**Figure 7*c***). The simulation that includes a reconstruction of bedrock elevation that accounts for the change in dynamic topography since 3 Ma leads to an ∼400-km retreat of the EAIS in the Wilkes Basin sector and brings the results of Pliocene ice sheet modeling into accord with the geological record from the offshore Antarctic margin (Cook et al. 2013; see also Mortimer et al. 2007). This retreat of ice is equivalent to a GMSL rise of 2 m. Sensitivity studies presented in Austermann et al. (2015) yielded a range of retreat distances (200–560 km) and contributions to GMSL rise (1.1–2.8 m).

We noted earlier that GIA at the grounding line of marine-based sectors of the ice sheet introduces a self-stabilization that mutes the advance and retreat of the ice sheet relative to model simulations that do not include an accurate treatment of ice age sea-level changes (Gomez et al. 2010, 2018). In contrast, the impact on ice sheet stability of dynamic topography at the grounding line depends on the sign of the topographic deflection: Subsidence of the crust will degrade the stability of an ice sheet, while uplift of the crust at the grounding line will enhance its stability. As reflected in **Figure 7**, the impact can be significant, and this suggests that modeling of ice

sheet evolution during other ice-house periods in Earth history must explore the potential effect of dynamic topography on bedrock elevation.

3. A ROLE FOR DYNAMIC TOPOGRAPHY IN THE INCEPTION OF NORTHERN HEMISPHERE GLACIATION

The long-term, secular cooling of Earth's climate through the Cenozoic is well established (Zachos et al. 2001), and critical events within this period, including the onset of glaciation in the Northern Hemisphere at ~2.7 Ma (e.g., Raymo 1994), remain an important focus of studies in ice age paleoclimate. The analysis of a deep-sea sedimentary core record from the North Atlantic (Shackleton et al. 1984) correlated the appearance of ice-rafted debris (IRD) with a negative oxygen isotope excursion at 2.4 Ma and thus established the presence of major continental ice sheets in the Northern Hemisphere at that time. Subsequent analyses of core records point to glaciation of various extent beginning at 2.7 Ma (Raymo et al. 1989, Jansen et al. 1990, Haug et al. 1999), or even earlier, at 3.4 Ma (Mudelsee & Raymo 2005).

However, while there is reasonable consensus on the timing of this onset, the mechanism(s) responsible for the climate transition from the MPWP to the Northern Hemisphere ice age cycles remain contentious. Climate perturbations associated with volcanism (Kennett & Thunell 1975); tectonic processes, including plateau uplift and increased weathering (Ruddiman & Kutzbach 1989, Raymo & Ruddiman 1992); and the closing of Panama Isthmus (e.g., Keigwin 1982, Haug & Tiedemann 1998) and Indonesian seaway (Cane & Molnar 2001) have been proposed as the main drivers of the event. The latter is related to more general arguments that the commencement of Northern Hemisphere glaciation followed the cessation of a stable, long-term El-Niño state (e.g., Philander & Fedorov 2003).

Climate modeling by Lunt et al. (2008) suggested that, with the exception of the impact of volcanism, which they did not consider, none of the above mechanisms acting alone, in combination, or in tandem with insolation variations was sufficient to trigger major glaciation in Greenland; instead, these authors argued that GIS glaciation was initiated by a reduction in atmospheric CO_2 concentration. A subsequent modeling study argued that a decrease in CO_2 concentration of ~100 ppm from 3.2 to 2.4 Ma was sufficient to explain various paleoclimate indicators (Willeit et al. 2015), consistent with an inference of CO_2 drawdown from an analysis of boron isotopes in planktic foraminifera in a sedimentary core spanning 4.6–2.0 Ma (Bartoli et al. 2011). The underlying cause of a CO_2 reduction of this magnitude is not clear from these studies, but Lunt et al. (2008) speculated that it may have been related to tectonics.

Donn & Shaw (1977) proposed that the Cenozoic cooling of North America, and the onset of ice age cycles in the region, was a result of a poleward migration of the continent associated with the combined effects of North American plate motion and movement of the rotation axis relative to the surface geography, known as true polar wander (TPW) (Goldreich & Toomre 1969). Their hypothesis appears to have been discounted in part because paleomagnetic inferences of Cenozoic TPW from the period (Jurdy & Van der Voo 1975) suggested that the process would have had a minor impact on climate. However, two recent studies based on a TPW path derived from a much larger paleomagnetic database have revived the idea (Steinberger et al. 2015, Daradich et al. 2017). **Figure 8*a*** shows the TPW path since the Late Cretaceous inferred by Doubrovine et al. (2012) and adopted in both studies. According to this reconstruction, polar wander has brought both North America and Greenland approximately 8° closer to the North Pole over the last 40 Myr. **Figure 8*b*** shows the combined impact of TPW and continental drift on paleogeography by superimposing the positions of North America and Greenland at both 30 Ma and the present day. A significant poleward migration of both landmasses is apparent on the figure.

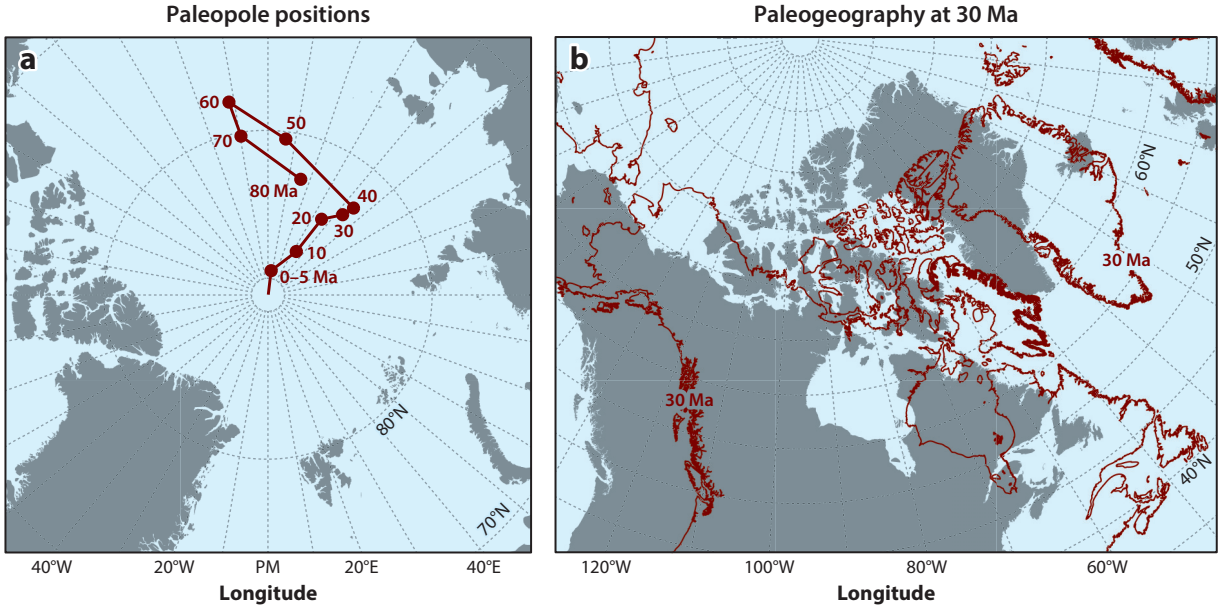

Figure 8

(*a*) Paleopole locations at 10-Myr intervals for the past 80 Myr (adapted from Doubrovine et al. 2012). (*b*) Paleogeography at 30 Ma (*red lines*) reconstructed by accounting for the true polar wander path in panel *a* and plate motions from GPlates (Müller et al. 2018). The present continental configuration is shown in light gray. Figure adapted from Daradich et al. (2017).

There is significant evidence that the onset of glaciation in the Northern Hemisphere occurred on Baffin Island rather than on Greenland. Hall & King (1989) argue for the initiation of ice rafting in Baffin Bay at ~3.4 Ma based on rock-magnetic stratigraphy of Ocean Drilling Project core 645, which revealed a change in sedimentation and the appearance of IRD at the site. Moreover, Birchfield et al. (1982) used a climate model adapted from Suarez & Held (1979) to argue that the high elevation in parts of Baffin Island made the area susceptible to glacial inception by increasing the local sensitivity to insolation forcing. It is also worth noting that there is strong consensus, from both sediment core records (Clark et al. 1993) and high-resolution, regional climate modeling (Birch et al. 2017), that Baffin Island was the inception site for North American glaciation at the end of the LIG (~116 ka).

Steinberger et al. (2015) argued that TPW and continental drift preconditioned glacial inception in Greenland at ~3 Ma, while Daradich et al. (2017) posited the same argument for Baffin Island. Moreover, Daradich et al. (2017) presented the results of a simple climate model that demonstrated that the secular reduction in insolation forcing driven by the poleward migration of Baffin Island in **Figure 8*b***, as measured by a change in average annual sum of positive-degree days, was comparable in magnitude to the forcing associated with obliquity and precession variations.

Steinberger et al. (2015) introduced a third factor that primed Greenland for glaciation at 3 Ma, namely, dynamic topography. Specifically, they reconstructed dynamic tomography variations by backward-advecting the governing equations of mantle flow using a suite of paired density and viscosity models that were tuned to provide good fits to surface observables, including heat flow, geoid variations, and present-day dynamic topography. Their prediction of the change in dynamic topography over the past 5 Ma, based on a model with density heterogeneity prescribed from the global seismic tomography model of Grand (2002), is shown in **Figure 9**. The high

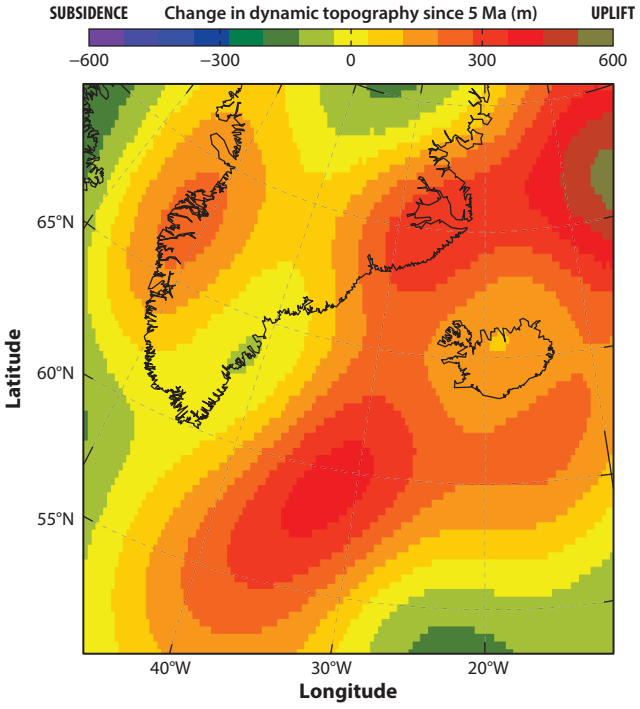

Figure 9

Dynamic topography change since 5 Ma computed by Steinberger et al. (2015) from a density and viscosity model based on the seismic tomography model of Grand (2002). Square-root-age law for topography away from the ridge has been subtracted out of this field. Figure adapted from Steinberger et al. (2015).

amplitude (∼300 m or ∼60 m/Myr) uplift on the eastern sector of Greenland predicted in the model is driven by hot upwelling flow in the North Atlantic that rises below Iceland and is then channeled northward toward Greenland by a zone of thinned lithosphere. This anomalously hot material in the shallow mantle has also been implicated as the driver of high geothermal heat flux and melting at the base of the ice sheet (Rogozhina et al. 2016). Steinberger et al. (2015) argue that this dynamically supported uplift is a third factor that preconditioned glacial inception on Greenland.

Coulson et al. (2018) performed simulations of dynamic topography over the Canadian Arctic through a backward-advected mantle convection simulation. Uplift in this region would have a number of effects on climate that would favor glacial inception, including an increase in the sensitivity of the region to insolation variations (Birchfield et al. 1982). **Figure 10** shows predictions of dynamic topography since 5 Ma based on four convection simulations. The first two adopt the TX2008 density model (Simmons et al. 2009) paired with the V1 and V2 mantle viscosity profiles (Mitrovica & Forte 2004). The remaining two Earth models are based on parameters described in Steinberger (2016) and the seismic tomography models S40RTS (Ritsema et al. 2011) and SAVANI (Auer et al. 2014). The conversion of these tomographic models to density and their accompanying viscosity profiles (which we denote as S16A and S16B, respectively) were tuned to fit large-scale surface observables related to mantle convection. Three of the four simulations predict an uplift of 75–150 m in northern Baffin Island over this time period (i.e., up to 30 m/Myr).

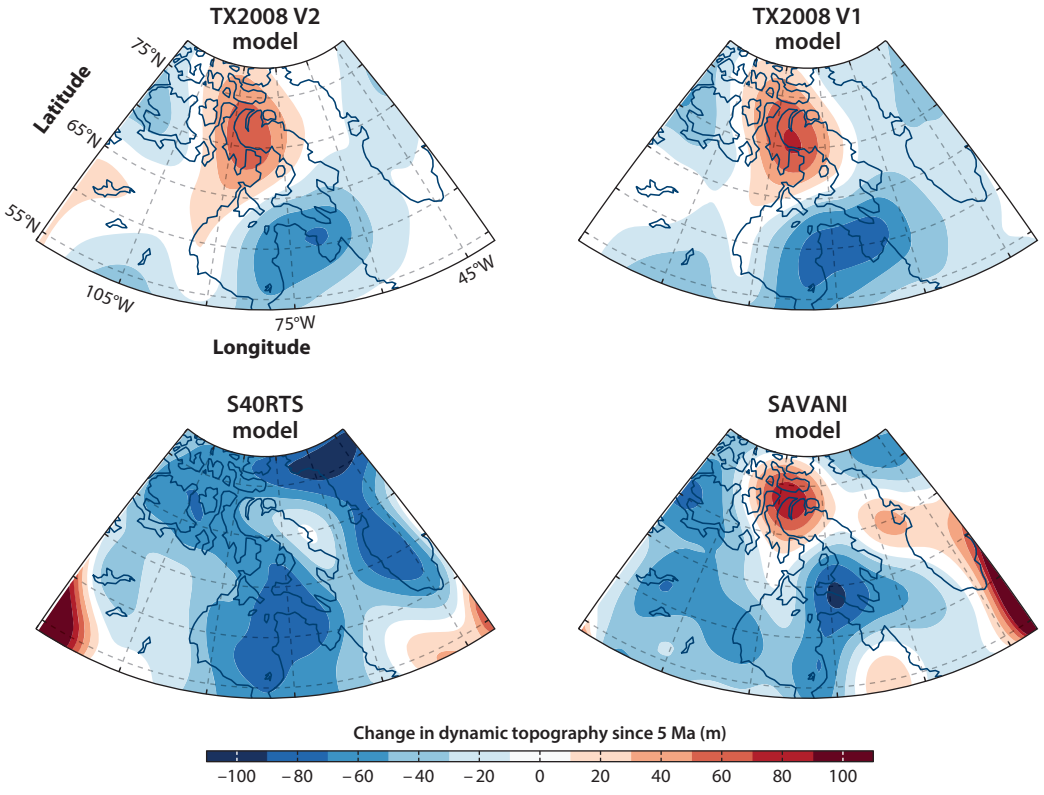

Figure 10

Predictions of dynamic topography change since 5 Ma based on four Earth models that are tuned to provide fits to a suite of surface observations related to mantle convection and additionally, in the case of the top row, observations of glacial isostatic adjustment (see text). Figure adapted from Coulson et al. (2018).

These predictions are consistent with the geological record, which indicates that mountain ranges and peneplains have been uplifted across Baffin Island since the late Cenozoic (Eyles 1996).

Dynamic topography over the high-latitude North Atlantic and Arctic may have played an additional role in glacial inception. In particular, Parnell-Turner et al. (2015) suggested that temporal variations in the thermal source of the Icelandic plume may have led to variable dynamic topography on the Greenland-Iceland–Faroe Ridge Complex (GIFRC). They speculated that uplift of the ridge system in the late Pliocene may have inhibited deep water flowing south from both the Denmark Strait to the northwest of Iceland and the Norwegian Sea to the east, impacting the Atlantic Meridional Overturning Circulation and cooling regional climate. We return to this hypothesis below since it has implications for global climate through the entire Neogene.

Quantifying the impact of dynamic topography over Greenland, Baffin Island, or the GIFRC on climate and exploring the role of the process on the inception of glaciation at ~3 Ma in these regions will require climate modeling of the kind discussed by Daradich et al. (2017) or the more sophisticated regional climate modeling of Birch et al. (2017). However, as with the myriad other processes proposed as the driver(s) of the inception, including the oft-cited connection of the event to the closing of the Panama Isthmus, a rigorous assignment of cause and effect remains challenging (Molnar 2008).

4. THE SIGNAL OF DYNAMIC TOPOGRAPHY IN LAST INTERGLACIAL SEA-LEVEL MARKERS

Of all efforts to consider analogs in paleoclimate archives for inferring the stability of polar ice sheets in our warming world, the LIG period, also known as MIS 5e or the Eemian, has received the most attention. The LIG extended from ~130 to 116 ka, during which global mean temperature and polar temperatures peaked 1–2 and ~5°C higher, respectively, than preindustrial levels (Andersen et al. 2004, Overpeck et al. 2006, Church et al. 2013). In a statistical study of a broad and geographically distributed suite of sea-level indicators, including corals, biological facies, geomorphological features, and oxygen isotope records, Kopp et al. (2009, 2013) concluded that peak GMSL reached ~6–9 m higher than present day. In an independent study of coral records, Dutton & Lambeck (2012) bounded peak GMSL during the LIG to 5.5–9 m, where the lower bound was based on records from western Australia and the upper bound on observations from the Seychelles. A reanalysis of the Seychelles record using a gravitationally self-consistent treatment of sea-level change associated with ice sheet melting during the LIG reduced this upper bound estimate to 7.5 m (Hay et al. 2014).

These published ranges are based on analyses that have accounted for the signal associated with GIA in response to the last few ice age cycles, and they reflect to varying extents the residual geographic variability in local sea-level highstands after correction for this effect. This variability raises two related questions. First, is the uncertainty in peak GMSL implied by these estimates a result of inadequacies in the adopted GIA corrections, or have other important processes contaminated the local sea-level records? Second, if unmodeled processes exist, will their identification refine these estimates of peak GMSL during the LIG or lead to additional uncertainty? The results summarized in Section 2 suggest that a candidate for study in this regard is dynamic topography. In particular, the investigations of both the Atlantic coastal plain of the United States (Rowley et al. 2013) and the Wilkes Basin (Austermann et al. 2015) suggest rates of dynamic topography generation at a level of several meters per 100 kyr at some sites since the mid-Pliocene, and such rates are clearly sufficient to impact estimates of peak GMSL during the LIG.

Austermann et al. (2017) published the first analysis of the potential impact of dynamic topography on local sea-level records dated to the LIG. The study considered sea-level indicators at 298 sites located on passive margins or on ocean islands without active volcanism that were culled from a larger global database (Ferranti et al. 2006, Kopp et al. 2009, Pedoja et al. 2014, Hibbert et al. 2016) (**Figure 11*a***). These indicators included coral reefs, marine terraces (i.e., a wave-cut rock ledge), beach ridges (i.e., a wave-swept or deposited sand or pebble ridge), and beach-related deposits (**Figure 11*b***). **Figure 12*a*** shows the distribution of elevations in the database constructed by sampling their indicative meaning (the relation between the elevation of the indicator and sea level in the modern context, including uncertainty). A decomposition of this distribution into contributions from each of the four classes of observation (**Figure 12*b–e***) indicates that the long, low-elevation tail in the former arises from submerged coral records, while the bump at 20 m elevation is primarily due to a set of marine terraces and beach ridges found at higher elevation. The expectation is that corrections to these distributions associated with postdepositional processes (e.g., GIA and dynamic topography) should bring them into closer accord, and any residual discordance might reflect inaccuracies in these corrections, estimates of indicative meaning, or relative differences in preservation bias.

Austermann et al. (2017) performed a set of 12 numerical simulations of dynamic topography based on combining each of the four Earth models described above—TX2008/V1, TX2008/V2, S40RTS/S16A, and SAVANI/S16B—with three different treatments of the horizontal flow velocity condition at the top of the convecting system—free-slip, no-slip, and present-day plate velocities taken from Seton et al. (2012). Given the relatively short timescale of interest, the predicted

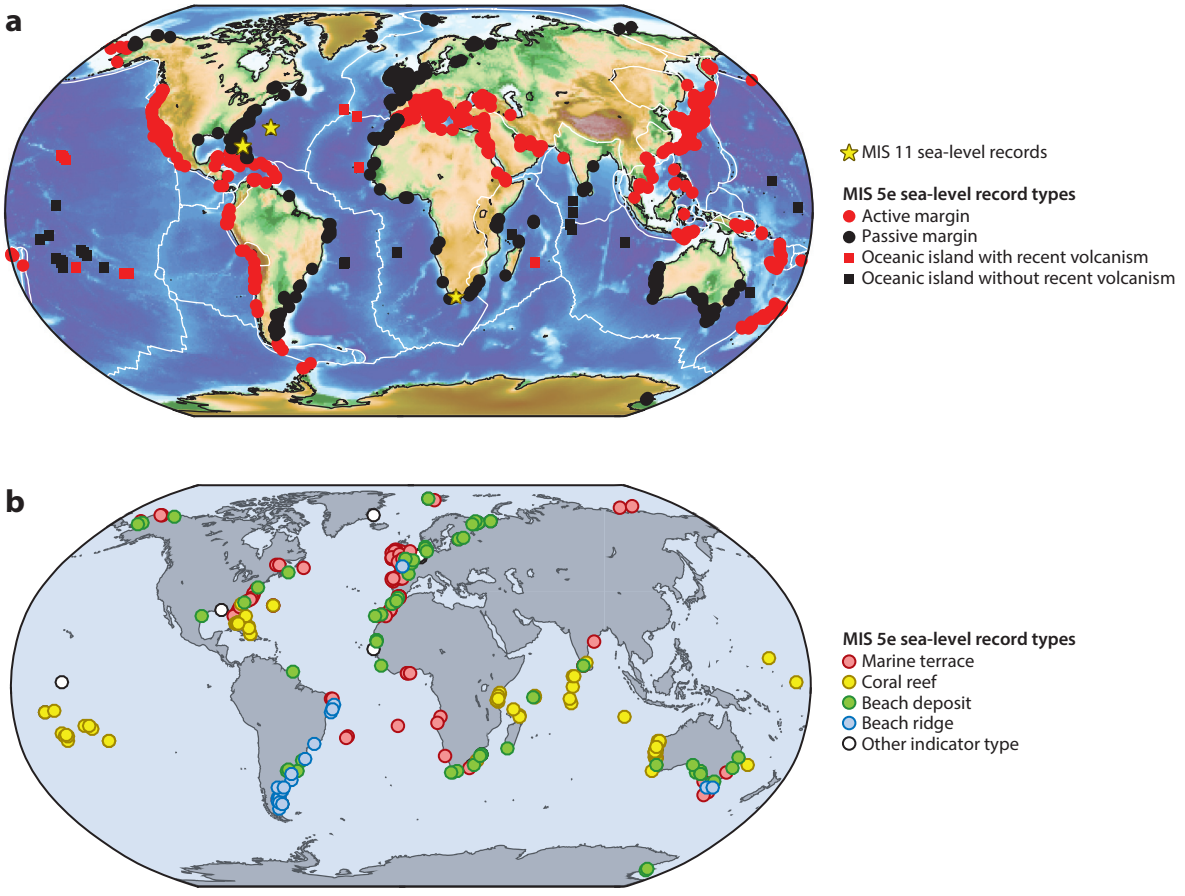

Figure 11

(*a*) Location of sea-level indicators of Last Interglacial age. Red symbols indicate sites located on active margins (*round*) and on oceanic islands with recent volcanic activity (*square*). Black symbols indicate sites located on passive margins (*round*) or ocean islands without recent volcanic activity (*square*). Red sites are removed from the analysis. Yellow stars are locations of Marine Isotope Stage (MIS) 11 sea-level records. White lines denote plate boundaries. (*b*) Sites in panel *a* (*black symbols*) color coded to show sea-level indicator type. Figure adapted from Austermann et al. (2017).

rate of change in dynamic topography moving forward in time was assumed to be the same as the rate since the LIG, and backward advection was thus avoided. Plots of the mean change in dynamic topography over the past 125 ka computed from the 12 simulations, and the associated standard deviation, are shown in **Figure 13*a*** and ***b***, respectively. There are noteworthy consistencies between these dynamic topography predictions and observations (**Figure 13*c***), including the tilt toward Tasmania to easternmost Australia (Sandiford 2007), the high elevation of Angola (Winterbourne et al. 2009), and the anomalously low elevations stretching from the southern tip of India to the Maldives.

The highest correlation between the observed elevation of the sea-level indicators and the dynamic topography predictions is achieved by the S40RTS/S16A and SAVANI/S16B Earth models run with no-slip and free-slip velocity (upper) boundary conditions (Austermann et al. 2017). The right column in **Figure 12** shows the various distributions on the left column after correction for this set of four simulations, and each panel provides the correlation coefficient between the

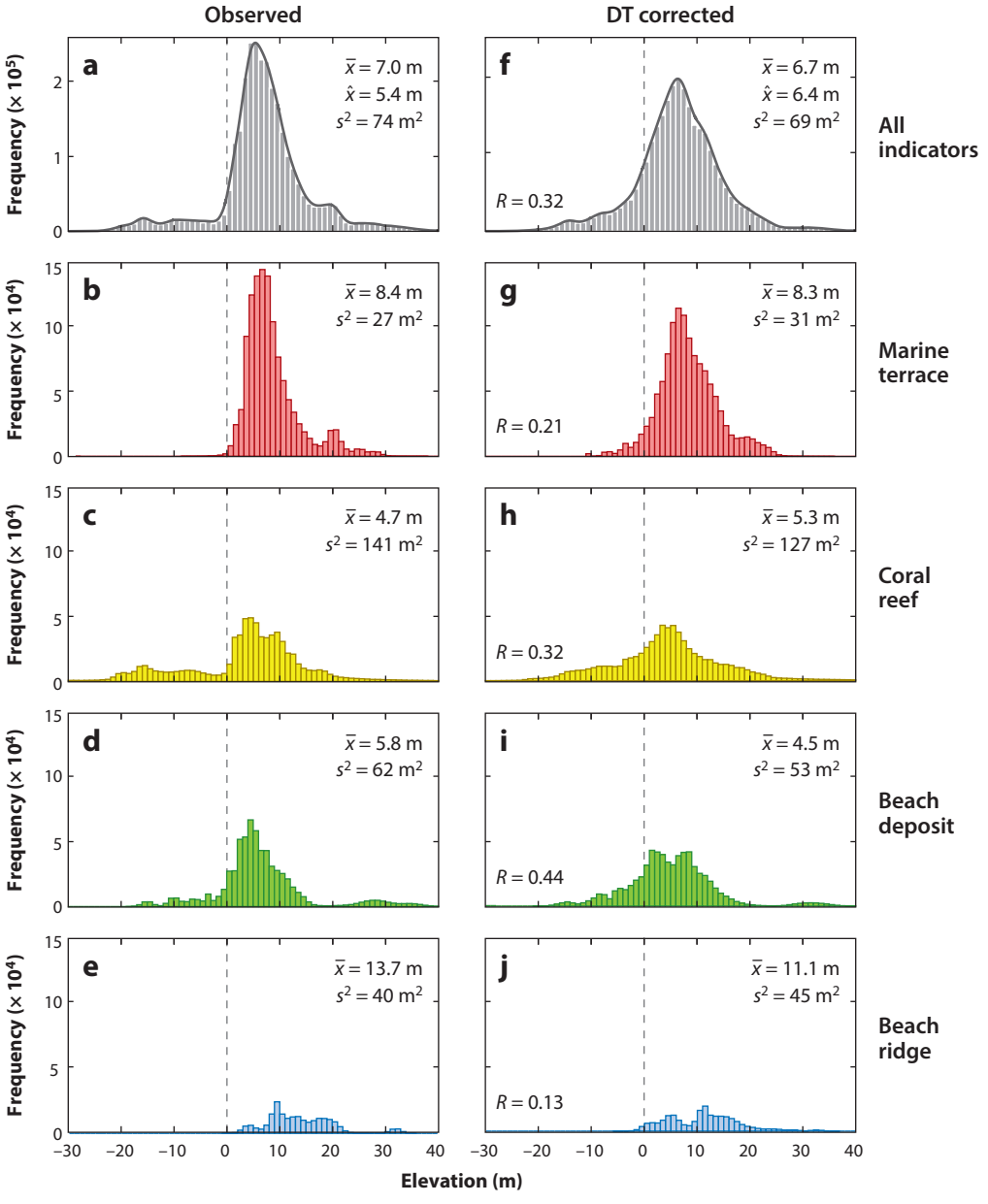

Figure 12

Distributions of observed sea-level highstands before (*left*) and after (*right*) correction for dynamic topography (DT). The distributions are constructed by drawing 10,000 samples from the uncertainty (indicative) range of the sea-level indicators used in the analysis (*black symbols* in **Figure 11*a***). The top row shows the results when all the data are considered, and the remaining rows repeat the analysis for individual data types, as labeled. The mean and variance of the distributions are listed on each panel, and the top panels also specify the maximum likelihood value. The DT corrections are based on 4 of the 12 simulations that individually yield the highest correlation between observations and predictions. The correlation between observations and predictions (R) based on this subset of convection simulations is provided on each of the panels at the right. Figure adapted from Austermann et al. (2017).

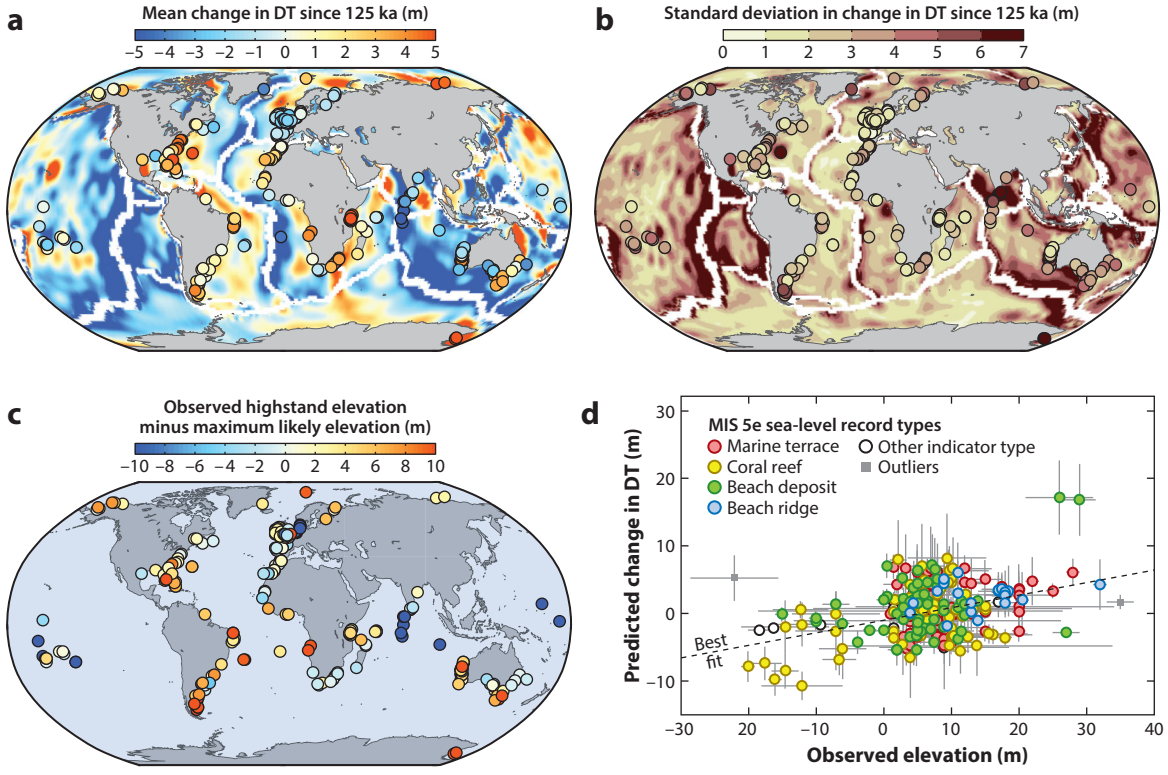

Figure 13

The (*a*) mean and (*b*) standard deviation of predictions of DT change since 125 ka computed from the 12 mantle convection simulations described in the text. The predictions account for the movement of each site in the local tectonic reference frame. White zones on each panel represent oceanic lithosphere of age less than 125 kiloyears. Circles indicate values at specific sites with Last Interglacial sea-level indicators (*black symbols* in **Figure 11**). (*c*) Observed highstand elevation at each site with the maximum likelihood estimate from **Figure 12*a*** (5.4 m) removed. (*d*) Predicted change in DT at each site versus the observed elevation of the sea-level indicator at that site. The prediction is based on the mean of the 4 mantle simulations out of 12 that individually yield the highest correlation between observations and predictions. Results are color coded to distinguish different subsets of sea-level indicators, as labeled. Abbreviations: DT, dynamic topography; MIS, Marine Isotope Stage. Figure adapted from Austermann et al. (2017).

observations and this set of four predictions. The corrected distribution for the full data set (**Figure 12*f***) has less skew and smaller variance than the raw data set. Moreover, the spread in the mean values across all four indicator types is also reduced from 9.0 m (4.7–13.7 m) for the uncorrected distributions to 6.6 m (4.5–11.1 m) for the corrected distributions. These metrics suggest a significant signal from dynamic topography, a conclusion confirmed by noting that the correlation coefficient for the entire data set (0.32; **Figure 12*f***) is significant at 95% confidence and the coefficients for all but the beach ridge data set are significant at 90% confidence. A detection of dynamic topography in the elevation of LIG sea-level markers is further demonstrated through a simple comparison between the predicted change in dynamic topography since 125 ka from the same set of four best-performing simulations and the observed elevations (**Figure 13*d***). The magnitude of the correlation is significant to 95% confidence.

This analysis raises several issues worthy of further consideration, as identified by Austermann et al. (2017). For example, as noted earlier, the spread of mean values associated with the various sea-level indicators (**Figure 12*g–j***) may point to a variable preservation bias among these data

types. Moreover, the best-fit slope in **Figure 13*d***, since it is significantly less than unity, indicates the presence of unmodeled signals in the observed highstands. This is not surprising given that the observations in the figure have not been corrected for the large and spatially variable signal of GIA in LIG sea level (Kopp et al. 2009, Lambeck et al. 2012). This signal is evident in the large magnitudes and high variability of the signal in **Figure 13*c*** at high-latitude sites covered by ice during the Last Glacial Maximum; however, an analysis in Austermann et al. (2017) suggests that other factors are involved in the low slope. These may include signals associated with sediment loading, limitations in the modeling of dynamic topography, data preservation issues, or inaccuracies in specifying the indicative meaning of each data type at each location.

The signal in **Figure 13*a*** includes a component associated with the subsidence of the oceanic lithosphere as it cools and moves away from the associated mid-ocean ridge. While the total prediction in **Figure 13*a*** is subject to numerous uncertainties associated with the adopted mantle density and viscosity fields and plate-mantle coupling, the change in the elevation of each site since 125 ka associated with plate cooling is far more accurately known. The latter signal is progressively smaller for islands on increasingly older lithosphere since the slope of the topography, which follows a square-root-age dependence, decreases with age, and it is perhaps surprising that a correction for this subsidence signal has only rarely been applied to LIG sea-level markers (e.g., Dickinson 2004). Austermann et al. (2017) demonstrate, for example, that the elevation of fossil coral reefs of LIG age is significantly correlated with the thermal subsidence signal at 90% confidence.

Is the detection of a dynamic topography signal in LIG sea-level indicators reported by Austermann et al. (2017) possible only by adopting a global database of observations from passive margins? Stephenson et al. (2019) argued that trends in the elevation of raised terraces in northern Madagascar reveal the existence of a significant signal from dynamic topography. **Figure 14** illustrates the LIG highstand elevations they obtained from field survey, which systematically decrease from a high of 9.3 m at the northernmost site (Cap d'Ambre) to 2.8 m at Irodo Bay, 80 km to the south. GIA modeling results they present predict a gradient of order 1 m in the opposite direction driven by ocean loading effects, and the authors conclude on this basis that the dominant contributor to the observed trend is dynamic topography. This argument is supported by evidence they cite of high uplift rates (exceeding 10 m/Myr) across northern Madagascar and seismic tomographic imaging of a relatively localized low-velocity anomaly beneath the region that may be rising.

Efforts to refine estimates of peak GMSL during the LIG on the basis of local sea-level indicators are motivated by the goal of understanding the stability of polar ice sheets in periods of climate warming. The results in **Figures 13*a*** and **14*b*** indicate that accuracy of these estimates will be limited to no better than 2–3 meters if corrections for dynamic topography are not incorporated into the analyses. This limitation is, of course, exacerbated as one considers earlier interglacials; for example, the dynamic topography signal will be a factor of ∼3–4 larger than the LIG signal in the case of the MIS 11 interglacial (420 ka), a period that has also been the focus of significant research (see Raymo & Mitrovica 2012, and references therein).

5. DYNAMIC TOPOGRAPHY AND ICE AGE PALEOCLIMATE: THINKING LONGER TERM

The analyses described above have focused on issues related to the Plio-Pleistocene. Here we extend our focus from the early Oligocene—the beginning of Earth's most recent ice-house period when ephemeral ice cover emerged in the Antarctic—to the Miocene by highlighting a broader set of studies linking dynamic topography to Cenozoic climate.

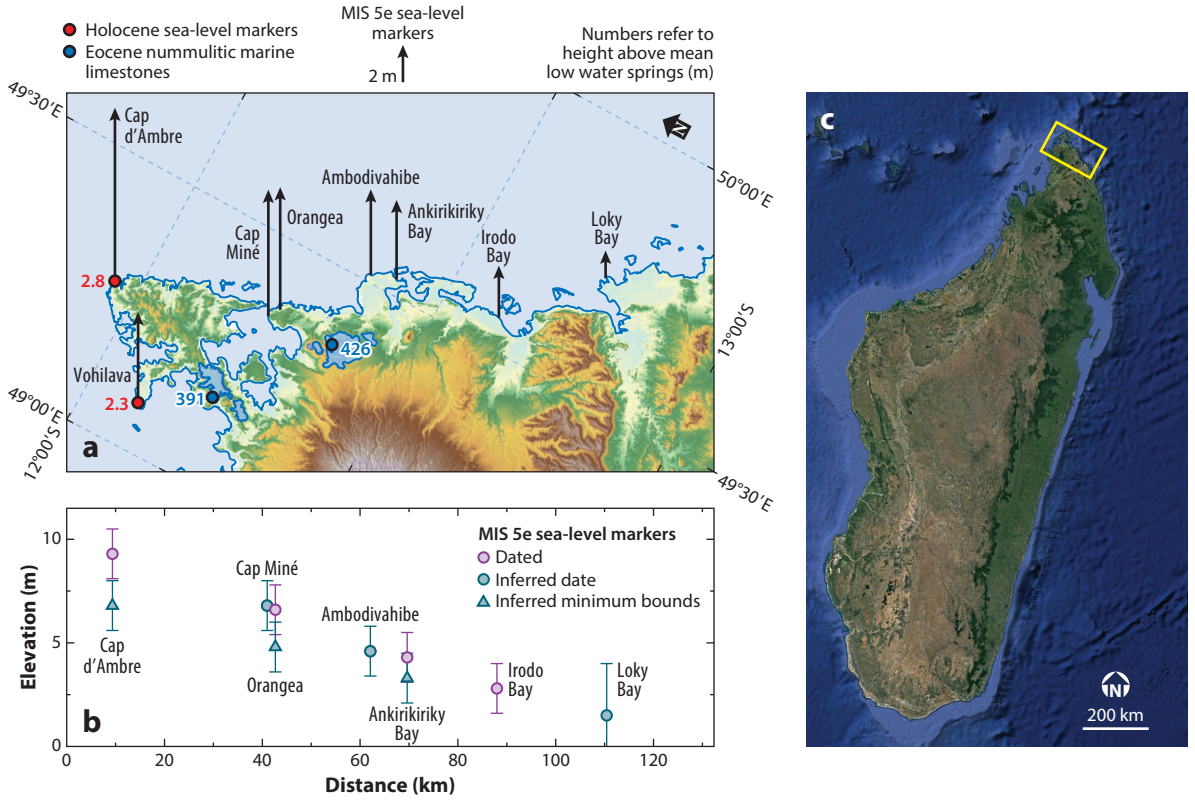

Figure 14

(*a*) Map of northern Madagascar showing locations of uplifted sea-level markers. Black arrows date from Last Interglacial, with length scaled by elevation above mean low water springs datum in meters. Blue polygons next to blue circles surround regions with outcrops of Eocene nummulitic limestones. Red circles are Holocene sea-level markers. (*b*) Transect from left to right along the northeast coastline showing elevations of Last Interglacial sea-level markers. (*c*) Map showing location of panel *a* (*yellow box*). Abbreviation: MIS, Marine Isotope Stage. Figure adapted from Stephenson et al. (2019).

The classic studies of Ruddiman & Kutzbach (1989) and Kutzbach et al. (1989) explored the impact of Cenozoic uplift of the western United States and the Tibetan Plateau on regional and global climate. While it was obvious to these authors that plate boundary deformation contributed to the development of topography in these regions, they were unaware of contemporaneous research demonstrating the central role of mantle flow in both of these well-documented epeirogenic events—in particular, subduction-controlled dynamic uplift of the western United States extending from the Rockies to the Great Plains (Mitrovica et al. 1989) and convective instability of the lithosphere as a driver for the uplift of the Tibetan Plateau (England & Houseman 1988).

Recent studies have brought a broad suite of observations to bear in establishing nuanced links between crustal uplift associated with dynamic topography, landscape evolution, and climate change. For example, Richards et al. (2016) argued that the broad, tilting toward the east of the Indian peninsula estimated from the pattern of residual age-depth anomalies in the surrounding ocean and constrained by the spatio-temporal pattern of eastward-draining rivers was driven by mantle flow. They speculated that the associated uplift of the Western Ghats mountain range may have influenced the intensity of the Indian monsoons in the Neogene. Furthermore, in a

comprehensive Earth systems study, Willett et al. (2018) demonstrated that dynamic topography in North America, as modeled by Moucha et al. (2008), led to an eastward migrating uplift front over the past 30 Ma that initially blanketed the High Plains with sediment fans that are now being progressively eroded by an actively evolving and migrating river network. Areas of the fans that are preserved have well-developed soils and inefficient drainage that has favored the development of wetlands in the form of playa lakes, and the authors argue that these have exerted a significant control on ecology and biodiversity.

Finally, we consider research exploring connections between dynamic topography and ocean chemistry and circulation that both record and impact paleoclimate variability. The carbonate compensation depth (CCD) represents a geographically variable surface within the ocean above which the supply of carbonate derived from the photic zone exceeds dissolution rates. The CCD is sensitive to changes in the rate of carbonate and silicate weathering of rocks on land and atmospheric CO_2 concentration (Raymo et al. 1988), as well as sea-level changes, and is thus an important metric for tracking the ocean carbon cycle and, more generally, long-term climate. Estimates of the CCD over time have been derived from the analysis of sedimentary cores under the assumption that paleodepth follows a simple model of thermal subsidence and sediment loading away from mid-ocean ridges. Campbell et al. (2018) have explored the impact of accounting for dynamic topography in reconstructions of paleodepths on estimates of CCD changes in the equatorial Pacific over the past 30 Myr. Their simulations of dynamic topography involve four Earth models that pair the TX2007 (Simmons et al. 2007) and TX2008 (Simmons et al. 2009) density models with the V1 and V2 viscosity profiles (Mitrovica & Forte 2004) described above. Incorporating dynamic topography into the analyses perturbs the estimate of CCD by ∼0.5 km by 30 Ma and leads to greater consistency with oxygen isotope variability (Zachos et al. 2008) over the same time window (**Figure 15**).

Next, we turn from ocean chemistry to ocean circulation and studies by Wright & Miller (1996), Poore et al. (2006), and Parnell-Turner et al. (2015). Variations in the Atlantic Meridional Overturning Circulation and the associated North Atlantic Deep Water (NADW) are thought to be important modulators of climate change (Buckley & Marshall 2016) and have been implicated, with some controversy, in driving a series of critical events in ice age climate. Overflow of water across the GIFRC represents an important source of NADW (**Figure 16**). This overflow is composed of Iceland-Scotland Overflow Water that passes over the Iceland–Faroe Ridge and the Faroe Bank Channel and Denmark Strait Overflow Water that flows through the passage between Iceland and Greenland.

Wright & Miller (1996) demonstrated that Neogene variations in the dynamic topography of these two gateways driven by changes in Iceland plume activity are correlated with variations in the flux of Northern Component Water (NCW, the proto-NADW). They used topographic profiles through the Reykjanes Ridge as a proxy for plume activity and estimated changes in water flux through a combination of benthic foraminiferal carbon isotope measurements in sediment cores and North Atlantic sedimentation patterns (Wright & Miller 1996). Poore et al. (2006) used carbon isotope measurements from a global database of cores to infer a significant increase in NCW flux from 6 to 2 Ma, which correlated with reduced plume support of topography on the GIFRC. Parnell-Turner et al. (2015) used stratigraphy within sediment deposits south of the ridge complex as a proxy for the flux of NCW and the bathymetry of V-shaped ridges straddling the Reykjanes Ridge as a proxy for plume activity and dynamic topography variations on the GIFRC. They added further support to the correlation suggested by Wright & Miller (1996), concluding that a reduction in plume activity and subsidence of the ridge complex increased water flux across these gateways from 5.5 to 2.5 Ma and that this trend subsequently reversed.

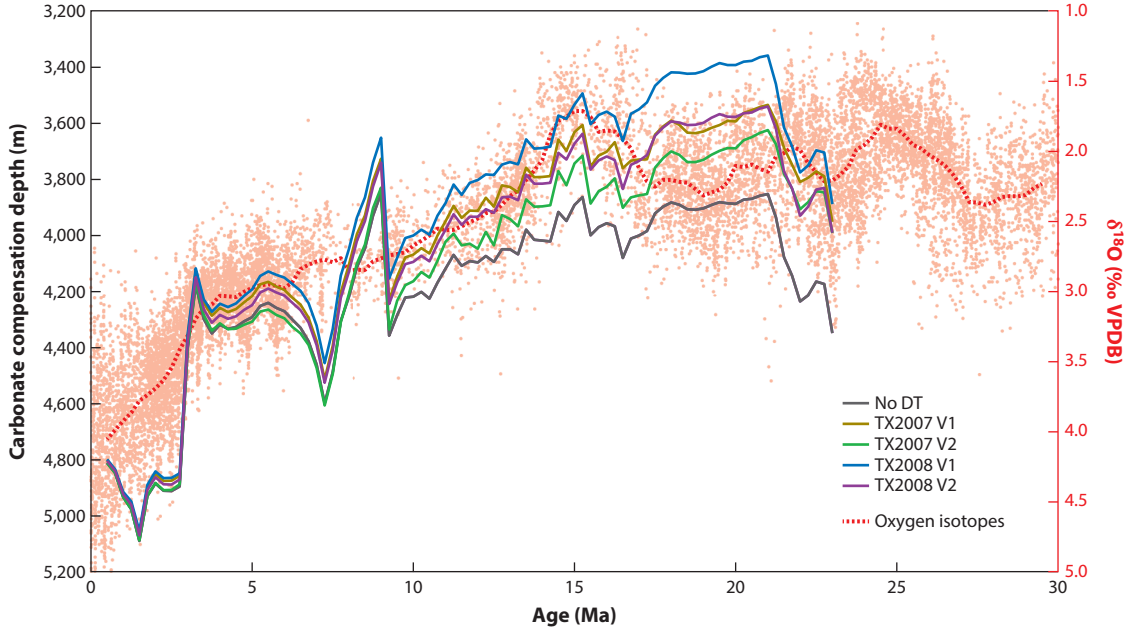

Figure 15

Carbonate compensation depth estimated by Campbell et al. (2018) from sedimentary cores in the equatorial Pacific with ocean paleodepth reconstructions corrected for DT using four different models and an estimate without such a correction (*dark gray line*). Red dots and running average (*dashed red line*) are oxygen isotope measurements reported by Zachos et al. (2008). Abbreviations: DT, dynamic topography; VPDB, Vienna Pee Dee Belemnite. Figure adapted from Campbell et al. (2018).

While the correlation between plume activity, dynamic topography of the GIFRC, and flux of the NCW proposed by these studies is compelling, the connection of regional or global climate to this variability is less persuasive. While Wright & Miller (1996) conclude that long-term climate through the Neogene was not controlled by variability in plume activity and NCW flux, they raise the possibility of a connection to a series of short-term climate perturbations from the early Miocene to middle Pliocene. Poore et al. (2006) and Parnell-Turner et al. (2015) both speculated that a reduction in NCW flux driven by a jump in plume activity and uplift of the GIFRC may have preconditioned the climate system sufficiently to trigger inception of glaciation in the Northern Hemisphere at 2.7 Ma (as discussed above). However, this argument appears to be inconsistent with their inference of a general reduction in plume flux until at least 2.5 Ma, and so to be correct it would require a short-term increase in plume activity at ~2.7 Ma that is unresolved in the various data sets they discuss, or it may reflect uncertainty in the geochronological control of these data.

6. FINAL REMARKS

Over the last 30 years, significant attention has been focused on the connections between dynamic topography and the geological expression of epeirogeny, and the many studies within this body of literature have moved back and forth from global- and continental-scale analyses of large-scale deformation to the modeling of localized geological expressions of mantle flow. The move from global to local scale was motivated and facilitated by progressive improvements in (*a*) the resolution of seismic tomographic imaging, which has revealed significant spectral power at short spatial

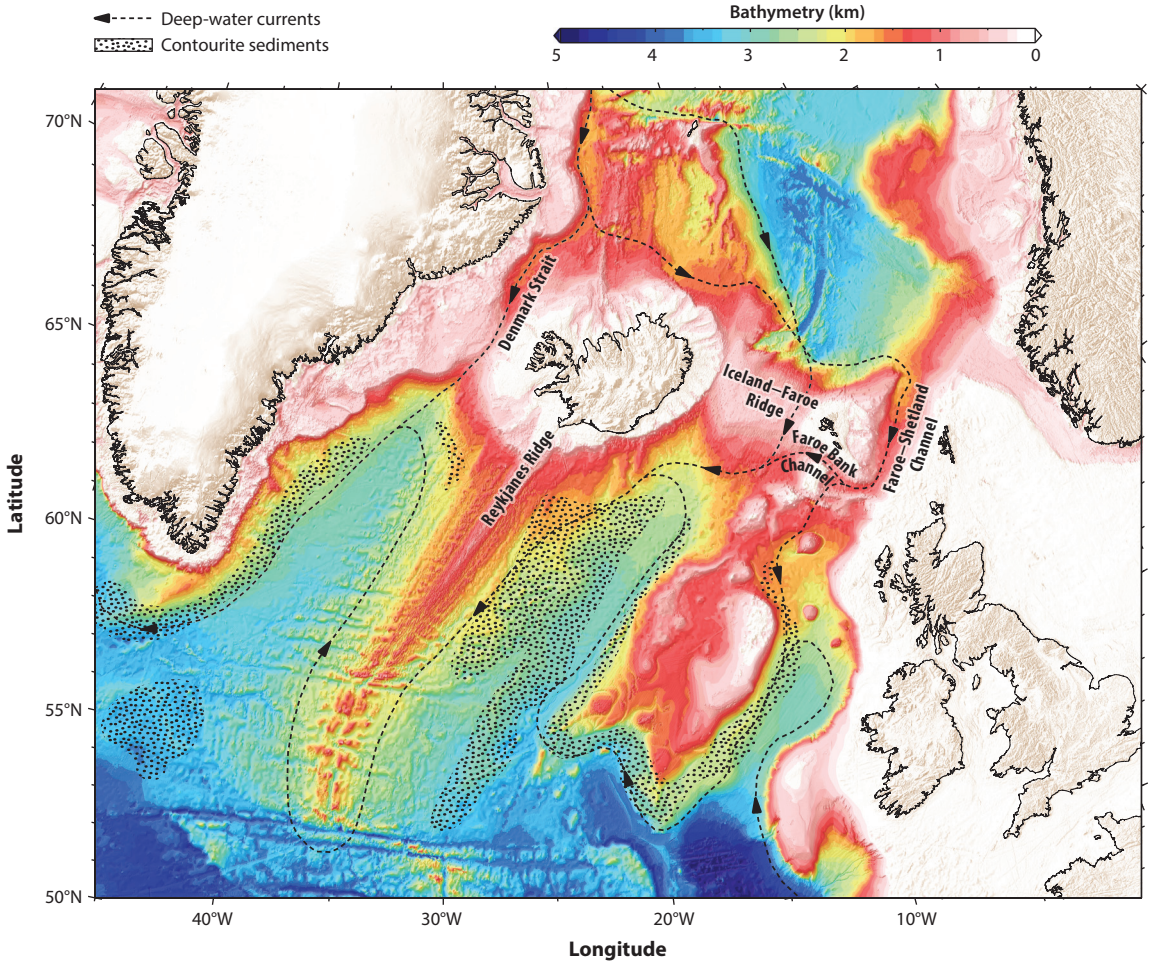

Figure 16

Present-day bathymetry of the North Atlantic region. Black arrows show the approximate locations of deep-water currents, including the overflow of North Atlantic Deep Water into the rest of the Atlantic circulation system. Stippled areas mark significant contourite deposits. Figure adapted from Parnell-Turner et al. (2015).

scales that is reflected in the associated predictions of dynamic topography; and (*b*) the sophistication of 3D numerical modeling of thermochemical convection, including methods that have been developed to turn the snapshot of seismic tomography into a movie marched back in geological time. The renewed interest in global studies reflects the recognition that key geological observations of the Earth system—for example, long-term, global-scale sea-level changes—represent an oceanwide integration of the dynamic topography field.

As these studies have progressively refined both spatial and temporal scales of dynamic topography observations and predictions, applications to paleoclimate have emerged (**Figure 17**). This review has focused on Plio-Pleistocene ice age climate, and we have highlighted research connecting the impact of dynamic topography fluctuations on ice sheet stability, including inception, and the elevation of ancient sea-level markers. However, we have also discussed studies with a broader range of timescales that explore the control of dynamic topography on continental-scale

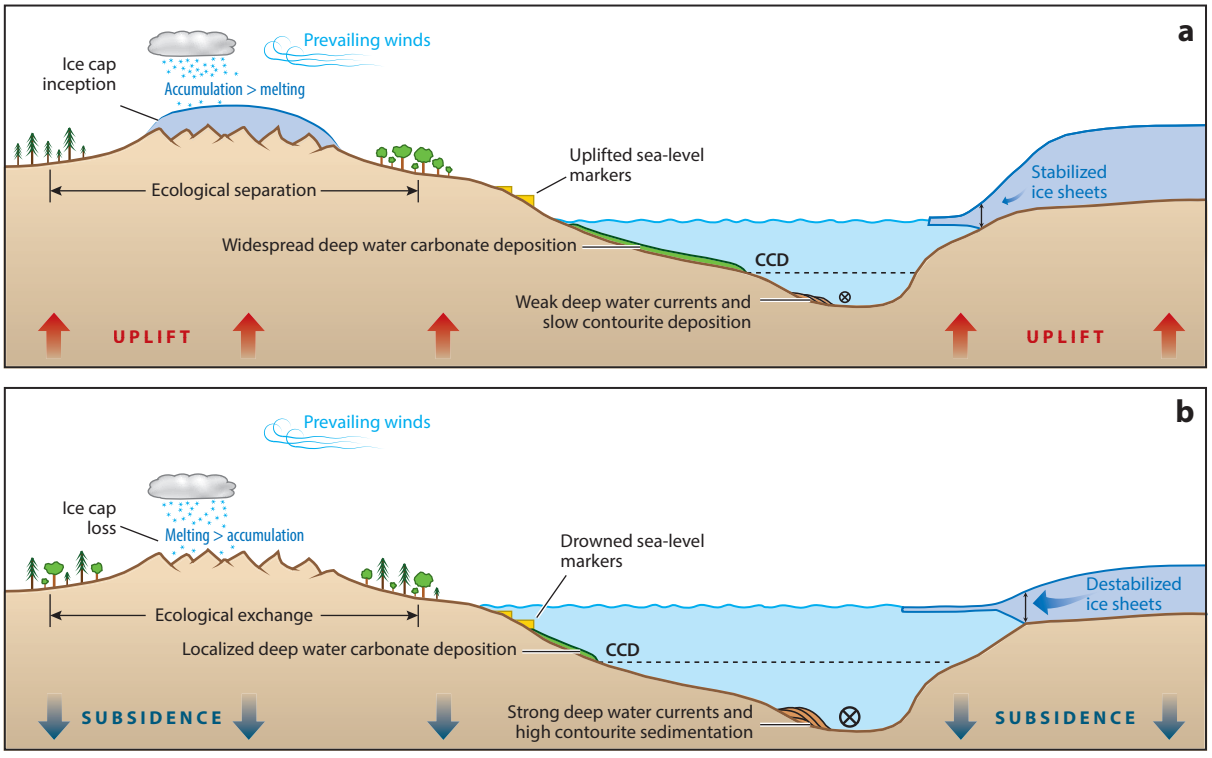

Figure 17

Schematic illustrating the impact of dynamic topography on a range of geological observables related to climate. The red and blue arrows at the base of each panel reflect the general direction of mantle flow responsible for crustal uplift or subsidence, respectively. Abbreviation: CCD, carbonate compensation depth.

ecology and biodiversity, deep water carbonate deposition (and associated estimates of the CCD), and water flux across oceanic gateways.

Many of the numerical modeling results in Sections 2–5—whether focused on the Plio-Pleistocene or not—are based on backward-advection simulations that extend back to the beginning of the Neogene or earlier. This raises two issues. First, the magnitude of dynamic topography changes predicted for the past 3 Myr, which can reach peak values of order 100 m or more, can increase over a longer geological time window by approximately an order of magnitude given that the timescale of convection within Earth's mantle is of order 100 Myr. This is important to keep in mind in sensitivity studies focused on more ancient ice-house periods in Earth history. Second, the accuracy of backward-advection schemes deteriorates in simulations that extend backward more than a few tens of Myr, and efforts to assess the impact of dynamic topography on ice age climate events dating, for example, to the early Oligocene may be well advised to move to more accurate, adjoint methods for performing retrodictions (e.g., Li et al. 2017, Ghelichkhan & Bunge 2018).

With few exceptions, this article has reviewed research in which modeling of dynamic topography has been applied to gain insight into specific climate events rather than research that used climate-based inferences of uplift to constrain dynamic topography (e.g., Conrad & Gurnis 2003). Some of the research we have highlighted has explained enigmatic evidence in the geological record of climate change—for example, the role of dynamic topography in driving instability of the Wilkes Basin sector of the EAIS during the MPWP; other case studies have deepened the

ongoing challenge of constraining key aspects of the ice age Earth system, such as estimating peak GMSL, or equivalently minimum ice volume, during the MPWP from local observations of sea-level highstands. However, all of these studies have broadened the admonition of Moucha et al. (2008) by demonstrating that there is no such thing as a stable platform even over ice age timescales. For this reason, geophysical modeling of solid Earth processes such as GIA and dynamic topography must remain a central consideration in paleoclimate studies.

DISCLOSURE STATEMENT

The authors are not aware of any affiliations, memberships, funding, or financial holdings that might be perceived as affecting the objectivity of this review.

ACKNOWLEDGMENTS

This article was supported by funding from Harvard University (J.X.M., S.C., M.J.H.), a Frank Knox Memorial Fellowship (S.C.), a Schmidt Science Fellowship (F.D.R.), and NASA Grant NNX17AE17G (J.X.M., M.J.H.). We thank the Computational Infrastructure for Geodynamics (**https://geodynamics.org**), which is funded by the National Science Foundation under award EAR-0949446 and EAR-1550901, for supporting the development of ASPECT. We also thank the PALSEA working group (**https://palseagroup.weebly.com**) and NSF (grant OCE-0825293 "PLIOMAX") for facilitating discussions related to this article at regular meetings.

LITERATURE CITED

Ackert RP, Kurtz MD. 2004. Age and uplift rates of Sirius Group sediments in the Dominion Range, Antarctica, from surface exposure dating and geomorphology. *Glob. Planet. Change* 42:207–25

Andersen KK, Azuma N, Barnola JM, Bigler M, Biscaye P, et al. 2004. High-resolution record of Northern Hemisphere climate extending into the last interglacial period. *Nature* 431:147–51

Auer L, Boschi L, Becker TW, Nissen-Meyer T, Giardini D. 2014. *Savani*: a variable resolution whole-mantle model of anisotropic shear velocity variations based on multiple data sets. *J. Geophys. Res. Solid Earth* 119:3006–34

Austermann J, Mitrovica JX. 2015. Calculating gravitationally self-consistent sea level changes driven by dynamic topography. *Geophys. J. Int.* 203:1909–22

Austermann J, Mitrovica JX, Huybers P, Rovere A. 2017. Detection of a dynamic topography signal in last interglacial sea-level records. *Sci. Adv.* 3:e1700457

Austermann J, Pollard D, Mitrovica JX, Moucha R, Forte AM, et al. 2015. The impact of dynamic topography change on Antarctic Ice Sheet stability during the mid-Pliocene warm period. *Geology* 43:927–30

Bangerth W, Dannberg J, Gassmoeller R, Heister T. 2014. ASPECT: Advanced Solver for Problems in Earth's ConvecTion. *Computational Infrastructure for Geodynamics Software*. **https://aspect.geodynamics.org/**

Bartoli G, Hönisch B, Zeebe RE. 2011. Atmospheric CO_2 decline during the Pliocene intensification of Northern Hemisphere glaciations. *Paleoceanography* 26:PA4213

Beaumont C. 1982. Platform sedimentation. In *Abstracts: Eleventh International Congress on Sedimentology, McMaster University, Hamilton, Ontario, Canada, August 22-27, 1982*. p. 132. Hamilton, Ont.: IAS Congress

Birch L, Cronin T, Tziperman E. 2017. Glacial inception on Baffin Island: the role of insolation, meteorology, and topography. *J. Clim.* 230:4047–64

Birchfield GE, Weertman J, Lunde AT. 1982. A model study of the role of high-latitude topography in the climatic response to orbital insolation anomalies. *J. Atmos. Sci.* 39:71–87

Braun J. 2010. The many surface expressions of mantle convection. *Nat. Geosci.* 3:825–33

Buckley MW, Marshall J. 2016. Observations, inferences, and mechanisms of Atlantic Meridional Overturning Circulation variability: a review. *Rev. Geophys.* 54:5–63

Campbell SM, Moucha R, Derry LA, Raymo ME. 2018. Effects of dynamic topography on the Cenozoic carbonate compensation depth. *Geochem. Geophys. Geosyst.* 19:1025–34

Cane MA, Molnar P. 2001. Closing of the Indonesian seaway as a precursor to east African acidification around 3–4 million years ago. *Nature* 411:157–62

Cao W, Flament N, Zahirovic S, Williams S, Müller RD. 2019. The interplay of dynamic topography and eustasy on continental flooding in the late Paleozoic. *Tectonophysics* 761:108–21

Christensen UR, Yuen DA. 1985. Layered convection induced by phase transitions. *J. Geophys. Res.* 90(B12):10291–300

Church JA, Clark PU, Cazenave A, Gregory JM, Jevrejeva S, et al. 2013. Sea level change. In *Climate Change 2013: The Physical Science Basis. Contribution of Working Group I to the Fifth Assessment Report of the Intergovernmental Panel on Climate Change*, ed. TF Stocker, D Qin, G-K Plattner, M Tignor, SK Allen, J Boschung, A Nauels, Y Xia, V Bex, PM Midgley, pp. 1137–216. New York: Cambridge Univ. Press

Clark PU, Clague JJ, Curry BB, Dreimanis A, Hicock SR, et al. 1993. Initiation and development of the Laurentide and Cordilleran ice sheets following the last interglaciation. *Quat. Sci. Rev.* 12:79–114

Clark PU, Dyke AS, Shakun JD, Carlson AE, Clark J, et al. 2009. The Last Glacial Maximum. *Science* 325:710–14

Clark PU, Pollard D. 1998. Origin of the middle Pleistocene transition by ice sheet erosion of regolith. *Paleoceanography* 13:1–9

Conrad CP. 2013. The solid Earth's influence on sea level. *Geol. Soc. Am. Bull.* 125:1027–52

Conrad CP, Gurnis M. 2003. Seismic tomography, surface uplift, and the breakup of Gondwanaland: integrating mantle convection backwards in time. *Geochem. Geophys. Geosyst.* 4:1031

Conrad CP, Husson L. 2009. Influence of dynamic topography on sea level and its rate of change. *Lithosphere* 1:110–20

Cook CP, van de Flierdt T, Williams T, Hemming SR, Iwai M, et al. 2013. Dynamic behaviour of the East Antarctic ice sheet during Pliocene warmth. *Nature* 6:765–69

Coulson S, Austermann J, Hoggard M, Richards F, Mitrovica JX. 2018. The role of dynamic topography on glacial inception in North America. Presented at AGU Fall Meet., Dec. 10–14, Washington, DC, Abstr. DI51B-0005

Creveling JR, Finnegan S, Mitrovica JX, Bergmann KD. 2018. Spatial variation in Late Ordovician glacioeustatic sea-level change. *Earth Planet. Sci. Lett.* 496:1–9

Creveling JR, Mitrovica JX. 2014. The sea-level fingerprint of Snowball Earth deglaciation. *Earth Planet. Sci. Lett.* 399:74–85

Czarnota K, Hoggard MJ, White NJ, Winterbourne J. 2013. Spatial and temporal patterns of Cenozoic dynamic topography around Australia. *Geochem. Geophys. Geosyst.* 14:634–58

Dansgaard W, Clausen HB, Gundestrup N, Hammer CU, Johnsen SF, et al. 1982. A new Greenland deep ice core. *Science* 218:1273–77

Daradich A, Huybers P, Mitrovica JX, Chan N-H, Austermann J. 2017. The influence of true polar wander on climate and glacial inception in North America. *Earth Planet. Sci. Lett.* 461:96–104

Daradich A, Mitrovica JX, Pysklywec RN, Willett S, Forte A. 2003. Mantle convection, dynamic topography and rift-flank uplift of Arabia. *Geology* 31:901–4

Daradich A, Pysklywec R, Mitrovica JX. 2002. Mantle flow modeling of the anomalous subsidence of the Silurian Baltic Basin. *Geophys. Res. Lett.* 29:20-1–4

de Boer B, Dolan AM, Bernales J, Gasson E, Goelzer H, et al. 2015. Simulating the Antarctic ice sheet in the late-Pliocene warm period: PLISMIP-ANT, an ice-sheet model intercomparison project. *Cryosphere* 9:881–903

DeConto RM, Pollard D, Kowalewski D. 2012. Modeling Antarctic ice sheet and climate variations during Marine Isotope Stage 31. *Glob. Planet. Change* 88:45–52

Denton GH, Sugden DE, Marchant DR, Hall BL, Wilch TI. 1993. East Antarctic Ice Sheet sensitivity to Pliocene climatic change from a Dry Valleys perspective. *Geogr. Ann.* 75:155–204

DiCaprio L, Gurnis M, Müller RD. 2009. Long-wavelength tilting of the Australian continent since the Late Cretaceous. *Earth Planet. Sci. Lett.* 278:175–85

Dickinson WR. 2004. Impacts of eustasy and hydro-isostasy on the evolution and landforms of Pacific atolls. *Palaeogeogr. Palaeoclimatol. Palaeoecol.* 213:251–69

Donn WL, Shaw DM. 1977. Model of climate evolution based on continental drift and polar wandering. *Geol. Soc. Am. Bull.* 88:390–96

Doubrovine PV, Steinberger B, Torsvik TH. 2012. Absolute plate motions in a reference frame defined by moving hot spots in the Pacific, Atlantic, and Indian oceans. *J. Geophys. Res.* 117(B9):B09101

Dowsett HJ, Cronin TM. 1990. High eustatic sea level during the middle Pliocene: evidence from the southeastern U.S. Atlantic Coastal Plain. *Geology* 18:435–38

Dowsett HJ, Dolan A, Rowley D, Moucha R, Forte AM, et al. 2016. The PRISM4 (mid-Piacenzian) paleoenvironmental reconstruction. *Clim. Past* 12:1519–38

Dutton A, Lambeck K. 2012. Ice volume and sea level during the Last Interglacial. *Science* 337:216–19

Dwyer GS, Chandler MA. 2009. Mid-Pliocene sea level and continental ice volume based on coupled benthic Mg/Ca palaeotemperatures and oxygen isotopes. *Philos. Trans. R. Soc. A* 367:157–69

Edwards TL, Brandon MA, Edwards NR, Golledge NR, Holden PB, et al. 2019. Revisiting Antarctic ice loss due to marine ice-cliff instability. *Nature* 566:58–64

England PC, Houseman GA. 1988. The mechanics of the Tibetan Plateau. *Philos. Trans. R. Soc. A* 326:301–20

Eyles N. 1996. Passive margin uplift around the North Atlantic region and its role in Northern Hemisphere late Cenozoic glaciation. *Geology* 24:103–6

Faccenna C, Rossetti F, Becker TW, Danesi S, Morelli A. 2008. Recent extension driven by mantle upwelling beneath the Admiralty Mountains (East Antarctica). *Tectonics* 27:TC4015

Ferranti L, Antonioli F, Mauz B, Amorosi A, Dai Pra G, et al. 2006. Markers of the last interglacial sea-level high stand along the coast of Italy: tectonic implications. *Quat. Int.* 145–146:30–54

Ferrier K, Austermann J, Mitrovica JX, Pico T. 2017. Incorporating sediment compaction into a gravitationally self-consistent model for ice age sea level change. *Geophys. J. Int.* 211:663–72

Flament N, Gurnis M, Müller RD. 2013. A review of observations and models of dynamic topography. *Lithosphere* 5:189–210

Forte AM, Mitrovica JX. 1997. A resonance in the Earth's obliquity and precession over the past 20 Myr driven by mantle convection. *Nature* 390:676–80

Forte AM, Peltier WR, Dziewonski AM, Woodward RL. 1993. Dynamic surface topography: a new interpretation based upon mantle flow models derived from seismic tomography. *Geophys. Res. Lett.* 20:225–28

Fretwell P, Pritchard HD, Vaughan DG, Bamber JL, Barrand NE, et al. 2013. Bedmap2: improved ice bed, surface and thickness datasets for Antarctica. *Cryosphere* 7:375–93

Ghelichkhan S, Bunge H-P. 2018. The adjoint equations for thermochemical compressible mantle convection: derivation and verification by twin experiments. *Proc. R. Soc. A* 474:20180329

Goldreich P, Toomre A. 1969. Some remarks on polar wandering. *J. Geophys. Res.* 74(10):2555–67

Gomez N, Latychev K, Pollard D. 2018. A coupled ice sheet–sea level model incorporating 3D Earth structure: variations in Antarctica during the last deglacial retreat. *J. Clim.* 31:4041–54

Gomez N, Mitrovica JX, Huybers P, Clark PU. 2010. Sea level as a stabilizing factor for marine-ice-sheet grounding lines. *Nat. Geosci.* 3:850–53

Gomez N, Pollard D, Mitrovica JX. 2013. A 3-D coupled ice sheet–sea level model applied to Antarctica through the last 40 ky. *Earth Planet. Sci. Lett.* 384:88–99

Grand SP. 2002. Mantle shear-wave tomography and the fate of subducted slabs. *Philos. Trans. R. Soc. A* 360:2475–92

Gurnis M. 1990. Ridge spreading, subduction, and sea level fluctuations. *Science* 250:970–72

Gurnis M. 1992. Rapid continental subsidence following the initiation and evolution of subduction. *Science* 255:1556–58

Gurnis M. 1993a. Comment on "Dynamic surface topography: a new interpretation based upon mantle flow models derived from seismic tomography," by A.M. Forte, W.R. Peltier, A.M. Dziewonski, and R.L. Woodward. *Geophys. Res. Lett.* 20:1663–64

Gurnis M. 1993b. Phanerozoic marine inundation of continents driven by dynamic topography above subducting slabs. *Nature* 364:589–91

Gurnis M, Mitrovica JX, Ritsema J, van Heijst HJ. 2000. Constraining mantle density structure using geological evidence of surface uplift rates: the case of the African Superplume. *Geochem. Geophys. Geosyst.* 1:1020

Gurnis M, Müller RD, Moresi L. 1998. Cretaceous vertical motion of Australia and the Australian-Antarctic discordance. *Science* 279:1499–504
Hager BH, Clayton RW, Richards MA, Comer RP, Dziewonski AM. 1985. Lower mantle heterogeneity, dynamic topography and the geoid. *Nature* 313:541–45
Hall FR, King JW. 1989. Rock magnetic stratigraphy of site 645 (Baffin Island) from ODP Leg 105. In *Proceedings of the Ocean Drilling Project, Scientific Results*, ed. FR Hall, JW King, SP Srivastava, MA Arthur, Clement MAB, pp. 843–62. College Station, TX: Ocean Drilling Program
Hambrey MJ, McKelvey B. 2000. Major Neogene fluctuations of the East Antarctic ice sheet: stratigraphic evidence from the Lambert Glacier region. *Geology* 28:887–90
Haug GH, Sigman DM, Tiedemann R, Pedersen TF, Sarnthein M. 1999. Onset of permanent stratification in the subarctic Pacific Ocean. *Nature* 401:779–82
Haug GH, Tiedemann R. 1998. Effect of the formation of the Isthmus of Panama on Atlantic Ocean thermohaline circulation. *Nature* 393:673–76
Hay C, Mitrovica JX, Gomez N, Creveling JR, Austermann J, Kopp RE. 2014. The sea-level fingerprints of ice-sheet collapse during interglacial periods. *Quat. Sci. Rev.* 87:60–69
Hayes JD, Pitman WC. 1973. Lithospheric plate motion, sea level changes and climatic and ecological consequences. *Nature* 246:18–22
Haywood AM, Hill DJ, Dolan AM, Otto-Bliesner BL, Bragg F, et al. 2013. Large-scale features of Pliocene climate: results from the Pliocene Model Intercomparison Project. *Clim. Past* 9:191–209
Heister T, Dannberg J, Gassmöller R, Bangerth W. 2017. High accuracy mantle convection simulation through modern numerical methods—II: realistic models and problems. *Geophys. J. Int.* 210:833–51
Hibbert FD, Rohling EJ, Dutton A, Chatcharavan PM, Zhao C, et al. 2016. Coral indicators of past sea-level change: a global repository of U-series dated benchmarks. *Quat. Sci. Rev.* 145:1–56
Hoggard MJ, White N, Al-Attar D. 2016. Global dynamic topography observations reveal limited influences of large-scale mantle flow. *Nat. Geosci.* 9:456–63
Hoggard MJ, Winterbourne J, Czarnota K, White N. 2017. Ocean residual depth measurements, the plate cooling model, and global dynamic topography. *J. Geophys. Res. Solid Earth* 122:2328–72
Holt WE, Stern TA. 1994. Subduction, platform subsidence, and foreland thrust loading: the late Tertiary development of the Taranaki Basin, New Zealand. *Tectonics* 13:1068–92
Huybers P. 2006. Early Pleistocene glacial cycles and the integrated summer insolation forcing. *Science* 313:508–11
James NP, Bone Y, Carter RM, Murray-Wallace CV. 2006. Origin of the late Neogene Roe Plains and their calcarenite veneer: implications for sedimentology and tectonics in the Great Australian Bight. *Aust. J. Earth Sci.* 53:407–19
Jansen E, Sjøholm J, Bleil U, Erichsen JA. 1990. Neogene and Pleistocene glaciations in the Northern Hemisphere and late Miocene–Pliocene global ice volume fluctuations: evidence from the Norwegian Sea. In *Geological History of the Polar Oceans: Arctic Versus Antarctic*, ed. U Bleil, J Thiede, pp. 677–705. New York: Springer
Jones AG, Afonso JC, Fullea J. 2017. Geochemical and geophysical constrains on the dynamic topography of the Southern African Plateau. *Geochem. Geophys. Geosyst.* 18:3556–75
Jurdy DM, Van der Voo R. 1975. True polar wander since the Early Cretaceous. *Science* 187:1193–96
Kaufman DS, Brigham-Grette J. 1993. Aminostratigraphic correlations and paleotemperature implications, Pliocene-Pleistocene high-sea-level deposits, northwestern Alaska. *Quat. Sci. Rev.* 12:21–33
Keigwin L. 1982. Isotopic paleoceanography of the Caribbean and East Pacific: role of Panama uplift in late Neogene time. *Science* 217:350–53
Kennett JP, Thunell RC. 1975. Global increase in Quaternary explosive volcanism. *Science* 187:497–503
Kopp RE, Simons FJ, Mitrovica JX, Maloof AC, Oppenheimer M. 2009. Global and local sea levels during the Last Interglacial: a probabilistic assessment. *Nature* 462:863–67
Kopp RE, Simons FJ, Mitrovica JX, Maloof AC, Oppenheimer MA. 2013. Probabilistic assessment of sea level variations within the last interglacial stage. *Geophys. J. Int.* 193:711–16
Krantz DE. 1991. A chronology of Pliocene sea-level fluctuations: the US Middle Atlantic Coastal Plain record. *Quat. Sci. Rev.* 10:163–74

Kronbichler M, Heister T, Bangerth W. 2012. High accuracy mantle convection simulation through modern numerical methods. *Geophys. J. Int.* 191:12–29

Kutzbach JE, Guetter PJ, Ruddiman WF, Prell WL. 1989. Sensitivity of climate to late Cenozoic uplift in southern Asia and the American west: numerical experiments. *J. Geophys. Res.* 94(D15):18393–407

Lambeck K, Purcell A, Dutton A. 2012. The anatomy of interglacial sea levels: the relationship between sea level and ice volumes during the Last Interglacial. *Earth Planet. Sci. Lett.* 315:4–11

Li D, Gurnis M, Stadler G. 2017. Towards adjoint-based inversion of time-dependent mantle convection with nonlinear viscosity. *Geophys. J. Int.* 209:86–105

Lisiecki LE, Raymo ME. 2005. A Pliocene-Pleistocene stack of 57 globally distributed benthic $\delta^{18}O$ records. *Paleooceanography* 20:PA1003

Lithgow-Bertelloni C, Gurnis M. 1997. Cenozoic subsidence and uplift of continents from time-varying dynamic topography. *Geology* 25:735–38

Lithgow-Bertelloni C, Silver PG. 1998. Dynamic topography, plate driving forces and the African superswell. *Nature* 395:269–72

Liu L, Gurnis M. 2010. Dynamic subsidence and uplift of the Colorado Plateau. *Geology* 38:663–66

Lunt DJ, Foster GL, Haywood AM, Stone EJ. 2008. Late Pliocene Greenland glaciation controlled by a decline in atmospheric CO_2 levels. *Nature* 454:1102–5

Lunt DJ, Haywood AM, Schmidt GA, Salzmann U, Valdes PJ, Dowsett HJ. 2010. Earth system sensitivity inferred from Pliocene modeling and data. *Nat. Geosci.* 3:60–64

Marple RT, Talwani PO. 2000. Evidence for a buried fault system in the Coastal Plain of the Carolinas and Virginia—implications for neotectonics in the southeastern United States. *Geol. Soc. Am. Bull.* 112:200–20

Masson-Delmotte V, Schulz M, Abe-Ouchi A, Beer J, Ganopolski A, et al. 2013. Information from paleoclimate archives. In *Climate Change 2013: The Physical Science Basis. Contribution of Working Group I to the Fifth Assessment Report of the Intergovernmental Panel on Climate Change*, ed. TF Stocker, D Qin, G-K Plattner, M Tignor, SK Allen, J Boschung, A Nauels, Y Xia, V Bex, PM Midgley, pp. 383–464. New York: Cambridge Univ. Press

Mayewski PA, Goldthwait RP. 1985. Glacial events in the Transantarctic Mountains: a record of the East Antarctic ice sheet. In *Geology of the Transantarctic Mountains. Antarctic Research Series*, ed. MD Turner, JF Splettstoesser, pp. 274–75. Washington, DC: Am. Geophys. Union

McKenzie DP, Roberts JM, Wiess NO. 1974. Convection in the Earth's mantle: towards a numerical simulation. *J. Fluid. Mech.* 62:465–538

Miller KG, Kominz MA, Browning JV, Wright JD, Mountain GS, et al. 2005. The Phanerozoic record of global sea-level change. *Science* 310:1293–98

Miller KG, Wright JD, Browning JV, Kulpecz A, Kominz M, et al. 2012. High tide of the warm Pliocene: implications for global sea level for Antarctic deglaciation. *Geology* 40:407–10

Mitrovica JX, Beaumont C, Jarvis GT. 1989. Tilting of continental interiors by the dynamical effects of subduction. *Tectonics* 5:1078–94

Mitrovica JX, Forte AM. 2004. A new inference of mantle viscosity based upon a joint inversion of convection and glacial isostatic adjustment data. *Earth Planet. Sci. Lett.* 225:177–89

Mitrovica JX, Pysklywec R, Beaumont C, Rutty A. 1996. The Devonian to Permian sedimentation of the Russian Platform: an example of subduction controlled long-wavelength tilting of continents. *J. Geodyn.* 22:79–96

Mitrovica JX, Tamisiea ME, Davis JL, Milne GA. 2001. Recent mass balance of polar ice sheets inferred from patterns of global sea-level change. *Nature* 409:1026–29

Molnar P. 2008. Closing of the Central American Seaway and the Ice Age: a critical review. *Paleoceanography* 23:PA2201

Mortimer N, Dunlap WJ, Isaac MJ, Sutherland RP, Faure K. 2007. Basal Adare volcanics, Robertson Bay, North Victoria Land, Antarctica: Late Miocene intraplate basalts of subaqueous origin. In *Antarctica: A Keystone in a Changing World*, ed. AK Cooper, CR Raymond. Washington, DC: Natl. Acad.

Moucha R, Forte AM. 2011. Changes in African topography driven by mantle convection. *Nat. Geosci.* 4:707–12

Moucha R, Forte AM, Mitrovica JX, Rowley DB, Quere S. 2008. Dynamic topography and long-term sea-level variations: There may be no such thing as a stable continental platform. *Earth Planet. Sci. Lett.* 271:101–8
Moucha R, Forte AM, Rowley DB, Mitrovica JX, Simmons NA, Grand SP. 2009. Deep mantle forces and the uplift of the Colorado Plateau. *Geophys. Res. Lett.* 36:L19310
Moucha R, Ruetenik GA. 2017. Interplay between dynamic topography and flexure along the U.S. Atlantic passive margin: insights from landscape evolution modeling. *Glob. Planet. Change* 149:72–78
Mudelsee M, Raymo ME. 2005. Slow dynamics of the Northern Hemisphere glaciation. *Paleoceanography* 20:PA4022
Müller RD, Cannon J, Qin X, Watson RJ, Gurnis M, et al. 2018. GPlates: building a virtual Earth through deep time. *Geochem. Geophys. Geosyst.* 19:2243–61
Müller RD, Sdrolias M, Gaina C, Steinberger B, Heine C. 2008. Long-term sea-level fluctuations driven by ocean basin dynamics. *Science* 319:1357–62
Naish TR, Wilson GS. 2009. Constraints on the amplitude of Mid-Pliocene (3.6–2.4 Ma) eustatic sea-level fluctuations from the New Zealand shallow-marine sediment record. *Philos. Trans. R. Soc. A* 367:169–87
Overpeck JT, Otto-Bliesner BL, Miller GH, Muhs DR, Alley RB, Kiehl JT. 2006. Paleoclimatic evidence for future ice-sheet instability and rapid sea-level rise. *Science* 311:1747–50
Pagani M, Liu ZH, LaRiviere J, Ravelo AC. 2010. High Earth-system climate sensitivity determined from Pliocene carbon dioxide concentration. *Nat. Geosci.* 3:27–30
Parnell-Turner R, White NJ, McCave IN, Henstock TJ, Murton B, Jones SM. 2015. Architecture of North Atlantic contourite drifts modified by transient circulation of the Icelandic mantle plume. *Geochem. Geophys. Geosyst.* 16:3414–35
Paxman G. 2019. *Reconstructing the palaeotopography of Antarctica*. PhD Thesis, Durham Univ., Durham, UK
Pedoja K, Husson L, Johnson ME, Melnick D, Witt C, et al. 2014. Coastal staircase sequences reflecting sea-level oscillations and tectonic uplift during the Quaternary and Neogene. *Earth Sci. Rev.* 132:13–38
Philander SG, Fedorov AV. 2003. Role of tropics in changing the response to Milankovich forcing some three million years ago. *Paleoceanography* 18:1045
Pico T, Mitrovica JX, Ferrier K, Braun J. 2016. Global ice volume during MIS 3 inferred from a sea level analysis of sedimentary core records in the Yellow River Delta. *Quat. Sci. Rev.* 152:72–79
Pohl A, Austermann J. 2018. A sea-level fingerprint of Late-Ordovician ice sheet collapse. *Geology* 46:595–98
Pollard D, DeConto RM. 2009. Modelling West Antarctic Ice Sheet growth and collapse through the past five million years. *Nature* 458:329–32
Pollard D, DeConto RM, Alley RB. 2015. Potential Antarctic Ice Sheet retreat driven by hydrofracturing and ice cliff failure. *Earth Planet. Sci. Lett.* 412:112–21
Poore HR, Samworth R, White NJ, Jones SM, McCave IN. 2006. Neogene overflow of northern component water at the Greenland-Scotland ridge. *Geochem. Geophys. Geosyst.* 7:Q06010
Pysklywec R, Mitrovica JX. 1998. Mantle flow mechanisms for the large-scale subsidence of continental interiors. *Geology* 26:687–90
Pysklywec R, Mitrovica JX. 1999. The role of subduction-induced subsidence in the evolution of the Karoo Basin. *J. Geol.* 107:155–64
Pysklywec R, Mitrovica JX. 2000. Mantle flow mechanisms of epeirogeny and their possible role in the evolution of the Western Canada Sedimentary Basin. *Can. J. Earth Sci.* 37:1535–48
Raymo ME. 1994. The initiation of Northern Hemisphere glaciation. *Annu. Rev. Earth Planet. Sci.* 22:353–83
Raymo M, Kozdon R, Evans D, Lisiecki L, Ford HL. 2018. The accuracy of mid-Pliocene δ^{18}O-based ice volume and sea level reconstructions. *Earth Sci. Rev.* 177:291–302
Raymo M, Mitrovica JX. 2012. Collapse of polar ice sheets during the stage 11 interglacial. *Nature* 483:453–56
Raymo ME, Mitrovica JX, O'Leary MJ, DeConto RM, Hearty PJ. 2011. Searching for eustasy in Pliocene sea-level records. *Nat. Geosci.* 4:328–32
Raymo ME, Oppo DW, Curry W. 1997. The Mid-Pleistocene climate transition: a deep sea carbon isotopic perspective. *Paleoceanography* 12:546–59
Raymo ME, Ruddiman WF. 1992. Tectonic forcing of late Cenozoic climate. *Nature* 359:117–22
Raymo ME, Ruddiman WF, Backman J, Clement BM, Martinson DG. 1989. Late Pliocene variation in Northern Hemisphere ice sheets and North Atlantic deep water circulation. *Paleoceanography* 4:413–46

Raymo ME, Ruddiman WF, Froelich PN. 1988. Influence of late Cenozoic mountain building on ocean geochemical cycles. *Geology* 16:649–52

Richards FD, Hoggard MJ, White NJ. 2016. Cenozoic epeirogeny of the Indian peninsula. *Geochem. Geophys. Geosyst.* 17:4920–54

Ritsema J, Deuss A, van Heijst HJ, Woodhouse JH. 2011. S40RTS: a degree-40 shear-velocity model for the mantle from new Rayleigh wave dispersion, teleseismic traveltime and normal-mode splitting function measurements. *Geophys. J. Int.* 184:1223–36

Rogozhina I, Petrunin AG, Vaughan APM, Steinberger B, Johnson JV, et al. 2016. Melting at the base of the Greenland ice sheet explained by Iceland hotspot history. *Nat. Geosci.* 9:366–72

Rovere A, Hearty PJ, Austermann J, Mitrovica JX, Gale J, et al. 2015. Mid-Pliocene shorelines of the US Atlantic Coastal Plain—an improved elevation database with comparison to Earth model predictions. *Earth-Sci. Rev.* 145:117–31

Rovere A, Raymo ME, Mitrovica JX, Hearty PJ, O'Leary MJ, Inglis JD. 2014. The Mid-Pliocene sea-level conundrum: glacial isostasy, eustasy and dynamic topography. *Geology* 387:27–33

Rowley DB, Forte AM, Moucha R, Mitrovica JX, Simmons NA, Grand SP. 2013. Dynamic topography change of the eastern United States since 3 million years ago. *Science* 340:1560–63

Ruddiman WF, Kutzbach JE. 1989. Forcing of late Cenozoic northern hemisphere climate by plateau uplift in southeast Asia and the American Southwest. *J. Geophys. Res.* 94(D15):18409–27

Sandiford M. 2007. The tilting continent: a new constraint on the dynamic topographic field from Australia. *Earth Planet. Sci. Lett.* 261:152–63

Scherer RP, DeConto RM, Pollard D, Alley R. 2016. Windblown Pliocene diatoms and East Antarctic Ice Sheet retreat. *Nat. Commun.* 7:12957

Sella G, Dixon TH, Mao A. 2002. REVEL: a model for recent plate velocities from space geodesy. *J. Geophys. Res.* 107(B4):ETG-11

Seton M, Müller RD, Zahirovic S, Gaina C, Torsvik T, et al. 2012. Global continental and ocean basin reconstructions since 200 Ma. *Earth-Sci. Rev.* 113:212–70

Shackleton NJ, Backman J, Zimmerman H, Kent DV, Hall MA, et al. 1984. Oxygen isotope calibration of the onset of ice-rafting and history of glaciation in the North Atlantic region. *Nature* 307:620–23

Shephard GE, Müller RD, Liu L, Gurnis M. 2010. Miocene drainage reversal of the Amazon River driven by plate-mantle interaction. *Nat. Geosci.* 3:870–75

Simmons NA, Forte AM, Grand SP. 2007. Thermochemical structure and dynamics of the African superplume. *Geophys. Res. Lett.* 34:L02301

Simmons NA, Forte AM, Grand SP. 2009. Joint seismic, geodynamic and mineral physical constraints on three-dimensional mantle heterogeneity: implications for the relative importance of thermal versus compositional heterogeneity. *Geophys. J. Int.* 177:1284–304

Soller DR. 1989. *Geology and tectonic history of the lower Cape Fear valley, southeastern North Carolina*. USGS Prof. Pap. 1466-A

Sosdian S, Rosenthal Y. 2009. Deep-sea temperature and ice volume changes across the Pliocene-Pleistocene climate transition. *Science* 325:306–10

Spasojevic S, Gurnis M. 2012. Sea level and vertical motion of continents from dynamic earth models since the Late Cretaceous. *AAPG Bull.* 96:2037–64

Spasojevic S, Gurnis M, Sutherland R. 2010. Inferring mantle properties with an evolving dynamic model of the Antarctica-New Zealand region from the Late Cretaceous. *J. Geophys. Res.* 115(B5):B05402

Spasojevic S, Liu L, Gurnis M, Müller RD. 2008. The case for dynamic subsidence of the U.S. east coast since the Eocene. *Geophys. Res. Lett.* 35:L08305

Steinberger B. 2016. Topography caused by mantle density variations: observation-based estimates and models derived from tomography and lithosphere thickness. *Geophys. J. Int.* 205:604–21

Steinberger B, Conrad CP, Tutu AO, Hoggard MJ. 2017. On the amplitude of dynamic topography at spherical harmonic degree two. *Tectonophysics* 760:221–28

Steinberger B, Spakman W, Japsen P, Torsvik TH. 2015. The key role of global solid-Earth processes in preconditioning Greenland's glaciation since the Pliocene. *Terra Nova* 27:1–8

Stephenson SN, White N, Li T, Robinson LF. 2019. Disentangling interglacial sea level and global dynamic topography: analysis of Madagascar. *Geochem. Geophys. Geosyst.* 519:61–69

Stroeven AP, Prentice MJ, Kleman J. 1996. On marine micro-fossil transport and pathways in Antarctica during the late Neogene: evidence from the Sirius Group at Mount Fleming. *Geology* 24:727–30

Suarez MJ, Held IM. 1979. The sensitivity of an energy balance climate model to variations in orbital parameters. *J. Geophys. Res.* 84(C8):4825–36

Wardlaw BR, Quinn TM. 1991. The record of Pliocene sea-level change at Enewetak Atoll. *Quat. Sci. Rev.* 10:247–58

Webb PN, Harwood DM, McKelvey BC, Mercer JH, Stott LD. 1984. Cenozoic marine sedimentation and ice-volume variation on the East Antarctic craton. *Geology* 12:287–91

Weertman J. 1974. Stability of the junction of an ice sheet and an ice shelf. *J. Glaciol.* 13:3–11

Wilch TI, Lux DR, Denton GH, McIntosh WC. 1993. Minimal Pliocene-Pleistocene uplift of the dry valleys sector of the Transantarctic Mountains: a key parameter in ice-sheet reconstructions. *Geology* 21:841–44

Willeit M, Ganopolski A, Calov R, Robinson A, Maslin M. 2015. The role of CO_2 decline for the onset of Northern Hemisphere glaciation. *Quat. Sci. Rev.* 119:22–34

Willett SD, McCoy SW, Beeson HW. 2018. Transience of the North American High Plains landscape and its impact on surface water. *Nature* 561:528–32

Wilson JT. 1965. A new class of faults and their bearing on continental drift. *Nature* 207:343–47

Winker CD, Howard JD. 1977. Correlation of tectonically deformed shorelines on the southern Atlantic coastal plain. *Geology* 5:123–27

Winterbourne J, Crosby A, White N. 2009. Depth, age and dynamic topography of oceanic lithosphere beneath heavily sedimented Atlantic margins. *Earth Planet. Sci. Lett.* 287:137–51

Wright JD, Miller KG. 1996. Greenland-Scotland ridge control of North Atlantic deep water. *Paleoceanography* 11:157–70

Yang T, Gurnis M. 2016. Dynamic topography, gravity and the role of lateral viscosity variations from inversion of global mantle flow. *Geophys. J. Int.* 207:1186–202

Zachos J, Dickens GR, Zeebe RE. 2008. An early Cenozoic perspective on greenhouse warming and carbon-cycle dynamics. *Nature* 451:279–83

Zachos J, Pagani M, Sloan L, Thomas E, Billups K. 2001. Trends, rhythms and aberrations in global climate 65 Ma to present. *Science* 292:68–72

Zahirovic S, Flament N, Dietmar Müller R, Seton M, Gurnis M. 2016. Large fluctuations of shallow seas in low-lying Southeast Asia driven by mantle flow. *Geochem. Geophys. Geosyst.* 17:3589–607

Zhang N, Zhong S, Flowers RM. 2012. Predicting and testing continental vertical motion histories since the Paleozoic. *Earth Planet. Sci. Lett.* 317:426–35

Annual Review
of Earth and
Planetary Sciences
Volume 48, 2020

Contents